

# Experimental Validation of a Rapid Assessment Tool for Pile Capacity and Stability in Response to Scour Situations

**Final Report**  
**October 2021**



---

**IOWA STATE UNIVERSITY**  
**Institute for Transportation**

**Sponsored by**  
Iowa Department of Transportation  
(InTrans Project 19-692)

## **About the Bridge Engineering Center**

The mission of the Bridge Engineering Center (BEC) is to conduct research on bridge technologies to help bridge designers/owners design, build, and maintain long-lasting bridges.

## **About the Institute for Transportation**

The mission of the Institute for Transportation (InTrans) at Iowa State University is to save lives and improve economic vitality through discovery, research innovation, outreach, and the implementation of bold ideas.

## **Iowa State University Nondiscrimination Statement**

Iowa State University does not discriminate on the basis of race, color, age, ethnicity, religion, national origin, pregnancy, sexual orientation, gender identity, genetic information, sex, marital status, disability, or status as a US veteran. Inquiries regarding nondiscrimination policies may be directed to the Office of Equal Opportunity, 3410 Beardshear Hall, 515 Morrill Road, Ames, Iowa 50011, telephone: 515-294-7612, hotline: 515-294-1222, email: eooffice@iastate.edu.

## **Disclaimer Notice**

The contents of this report reflect the views of the authors, who are responsible for the facts and the accuracy of the information presented herein. The opinions, findings and conclusions expressed in this publication are those of the authors and not necessarily those of the sponsors.

The sponsors assume no liability for the contents or use of the information contained in this document. This report does not constitute a standard, specification, or regulation.

The sponsors do not endorse products or manufacturers. Trademarks or manufacturers' names appear in this report only because they are considered essential to the objective of the document.

## **Iowa DOT Statements**

Federal and state laws prohibit employment and/or public accommodation discrimination on the basis of age, color, creed, disability, gender identity, national origin, pregnancy, race, religion, sex, sexual orientation or veteran's status. If you believe you have been discriminated against, please contact the Iowa Civil Rights Commission at 800-457-4416 or Iowa Department of Transportation's affirmative action officer. If you need accommodations because of a disability to access the Iowa Department of Transportation's services, contact the agency's affirmative action officer at 800-262-0003.

The preparation of this report was financed in part through funds provided by the Iowa Department of Transportation through its "Second Revised Agreement for the Management of Research Conducted by Iowa State University for the Iowa Department of Transportation" and its amendments.

The opinions, findings, and conclusions expressed in this publication are those of the authors and not necessarily those of the Iowa Department of Transportation.

**Technical Report Documentation Page**

<b>1. Report No.</b> InTrans Project 19-692	<b>2. Government Accession No.</b>	<b>3. Recipient's Catalog No.</b>	
<b>4. Title and Subtitle</b> Experimental Validation of a Rapid Assessment Tool for Pile Capacity and Stability in Response to Scour Situations		<b>5. Report Date</b> October 2021	
		<b>6. Performing Organization Code</b>	
<b>7. Author(s)</b> Zhengyu Liu (orcid.org/0000-0002-7407-0912), Katelyn S. Freeseaman (orcid.org/0000-0003-0546-3760), Brent M. Phares (orcid.org/0000-0001-5894-4774), and Seyedamin Mousavi (orcid.org/0000-0003-4203-8894)		<b>8. Performing Organization Report No.</b> InTrans Project 19-692	
<b>9. Performing Organization Name and Address</b> Bridge Engineering Center Iowa State University 2711 South Loop Drive, Suite 4700 Ames, IA 50010-8664		<b>10. Work Unit No. (TRAIS)</b>	
		<b>11. Contract or Grant No.</b>	
<b>12. Sponsoring Organization Name and Address</b> Iowa Department of Transportation 800 Lincoln Way Ames, IA 50010		<b>13. Type of Report and Period Covered</b> Final Report	
		<b>14. Sponsoring Agency Code</b> 19-SPR2-002	
<b>15. Supplementary Notes</b> Visit <a href="https://intrans.iastate.edu/">https://intrans.iastate.edu/</a> for color pdfs of this and other research reports.			
<b>16. Abstract</b> Concrete encasements are utilized to protect bridge piles from corrosion and environmental stressors. However, the contributions of concrete encasements in pile capacity are not considered in the design procedure. On the other hand, rating engineers need to have realistic evaluations of the piles to estimate the capacity of the foundation for scour-critical bridges. For this reason, a rapid assessment tool was developed in the Phase I research to calculate the capacity of concrete encased piles.  This rapid pile assessment tool was developed and verified using theoretical modeling approaches. However, experimental data to validate the tool's results were not available or included as part of that work. The goal of this research project was to validate the previously developed rapid pile assessment tool's findings to ensure accurate pile capacity determination, both for bare piles and those encased in concrete.  To achieve this goal, four specimens with various pile lengths and concrete encasement lengths and ratios were constructed and tested using axial loads in the laboratory. The results from the experimental test were compared with the predictions from the assessment tool. The results indicated that the pile assessment tool provides conservative estimation of the axial capacity of the piles. The prediction results were about 8% to 24% lower than those from the experimental results. Even more important is the fact that considering the encasement in capacity calculations can result in significantly higher available capacities.			
<b>17. Key Words</b> bridge pile capacity—concrete encasements—rapid assessment tool—scour-critical bridges		<b>18. Distribution Statement</b> No restrictions.	
<b>19. Security Classification (of this report)</b> Unclassified.	<b>20. Security Classification (of this page)</b> Unclassified.	<b>21. No. of Pages</b> 54	<b>22. Price</b> NA



# **EXPERIMENTAL VALIDATION OF A RAPID ASSESSMENT TOOL FOR PILE CAPACITY AND STABILITY IN RESPONSE TO SCOUR SITUATIONS**

**Final Report  
October 2021**

## **Principal Investigator**

Katelyn Freeseaman, Acting Director  
Bridge Engineering Center, Iowa State University

## **Co-Principal Investigators**

Zhengyu Liu, Research Engineer  
Brent M. Phares, Bridge Research Engineer  
Bridge Engineering Center, Iowa State University

## **Research Assistant**

Syedamin Mousavi

## **Authors**

Zhengyu Liu, Katelyn Freeseaman, Brent M. Phares, and Syedamin Mousavi

Sponsored by  
Iowa Department of Transportation  
(InTrans Project 19-692)

Preparation of this report was financed in part  
through funds provided by the Iowa Department of Transportation  
through its Research Management Agreement with the  
Institute for Transportation

A report from  
**Bridge Engineering Center**  
**Iowa State University**  
2711 South Loop Drive, Suite 4700  
Ames, IA 50010-8664  
Phone: 515-294-8103 / Fax: 515-294-0467  
<https://bec.iastate.edu/>



## TABLE OF CONTENTS

ACKNOWLEDGMENTS .....	vii
EXECUTIVE SUMMARY .....	ix
CHAPTER 1. INTRODUCTION .....	1
1.1 Background and Problem Statement.....	1
1.2 Objective .....	2
1.3 Report Content .....	2
CHAPTER 2. LITERATURE REVIEW .....	3
CHAPTER 3. LABORATORY TESTING .....	8
3.1 Test Design .....	8
3.2 Specimen Construction .....	9
3.3 Test Setup and Loading Configuration .....	10
3.4 Instrumentation Plans.....	12
3.4.1 Specimen-1 Instrumentation Plan .....	13
3.4.2 Specimen-2 Instrumentation Plan .....	15
3.4.3 Specimen-3 Instrumentation Plan .....	16
3.4.4 Specimen-4 Instrumentation Plan .....	18
3.4.5 Additional Instrumentation .....	20
3.5 Test Results .....	22
3.5.1 Specimen-1 Test Results.....	22
3.5.2 Specimen-2 Test Results.....	26
3.5.3 Specimen-3 Test Results.....	32
3.5.4 Specimen-4 Test Results.....	35
3.5.5 Results Summary .....	38
CHAPTER 4. ASSESSMENT TOOL VALIDATION .....	40
CHAPTER 5. SUMMARY AND CONCLUSIONS .....	41
REFERENCES .....	43

## LIST OF FIGURES

Figure 1. Vertical failure modes of bridge foundations .....	4
Figure 2. Steel H-pile concrete encasement for rehabilitation purposes used in Ohio .....	6
Figure 3. Steel H-piles with concrete encasement used in Iowa.....	6
Figure 4. Iowa DOT concrete encasement standard for H-piles.....	7
Figure 5. Specimen-3 and Specimen-4 .....	9
Figure 6. Test setup.....	10
Figure 7. Pile pin-end setup .....	11
Figure 8. Pin connection details.....	11
Figure 9. Pile fixity inside the concrete block .....	12
Figure 10. Instrumentation on Specimen-1 .....	13
Figure 11. Instrumentation on Specimen-2.....	15
Figure 12. Instrumentation on Specimen-3.....	17
Figure 13. Instrumentation on Specimen-4.....	19
Figure 14. Additional instrumentation .....	21
Figure 15. Deformed shape of Specimen-1 .....	22
Figure 16. Axial load-displacement of Specimen-1 .....	23
Figure 17. Strain data from Specimen-1 .....	24
Figure 18. Displacement data from Specimen-1.....	26
Figure 19. Deformed shape of Specimen-2 .....	27
Figure 20. Crack pattern in the concrete encasement of Specimen-2.....	28
Figure 21. Axial load-displacement of Specimen-2 .....	28
Figure 22. Strain data from Specimen-2 .....	30
Figure 23. Displacement data from Specimen-2.....	31
Figure 24. Deformed shape of Specimen-3 .....	33
Figure 25. Axial load-displacement of Specimen-3 .....	33
Figure 26. Strain data from Specimen-3 .....	34
Figure 27. Displacement data from Specimen-3.....	35
Figure 28. Deformed shape of Specimen-4 .....	36
Figure 29. Axial load-displacement of Specimen-4 .....	37
Figure 30. Strain data from Specimen-4.....	38
Figure 31. Displacement data from Specimen-4.....	38
Figure 32. Comparison of load-displacement from all specimens .....	39

## LIST OF TABLES

Table 1. Specimen details .....	8
Table 2. Material properties.....	9
Table 3. Instrumentation details for Specimen-1 .....	14
Table 4. Instrumentation details for Specimen-2.....	16
Table 5. Instrumentation details for Specimen-3.....	18
Table 6. Instrumentation details from Specimen-4.....	20
Table 7. Experimental buckling test results for all specimens.....	39
Table 8. Comparison between experimental and assessment tool results .....	40

## **ACKNOWLEDGMENTS**

The research team would like to thank the Iowa Department of Transportation (DOT) for sponsoring this work using state planning and research Federal SPR Part II, CFDA 20.205 funding. The authors would also like to thank members of the technical advisory committee for their contributions and direction.



## **EXECUTIVE SUMMARY**

Concrete encasements are utilized to protect bridge piles from corrosion and environmental issues. However, the contributions of concrete encasements are not traditionally considered in the design procedure. On the other hand, rating engineers need to have realistic evaluation methods for piles to estimate the capacity of the foundation for scour-critical bridges. For this reason, a rapid assessment tool was developed in the Phase I research to calculate the capacity of concrete encased piles.

This rapid pile assessment tool was developed and verified using theoretical modeling approaches. However, experimental data to validate the tool's results were not part of the scope for that study.

The goal of this research project was to validate the previously developed rapid pile assessment tool's findings to ensure accurate pile capacity determination, both for bare piles and those encased in concrete.

To achieve this goal, four specimens with various pile lengths and concrete encasement lengths and ratios were constructed and tested using axial loads in the laboratory. The results from the experimental tests were compared with the predictions from the assessment tool.

The results indicated that the pile assessment tool provides conservative estimation of the axial capacity of the piles with the prediction results approximately 8% to 24% lower than those from the experimental results. While the tool provides conservative estimations, the calculated capacities are still significantly higher than specification-based values, thus providing greater accuracy and capacity to rating engineers.



## **CHAPTER 1. INTRODUCTION**

### **1.1 Background and Problem Statement**

Concrete encasements are commonly used for bridge substructure piles that are exposed to the air or stream to protect them. This practice also provides additional stiffness to the piles. The unbraced length of the piles increases when scour reduces the presence of soil surrounding the piles. The resulting increase in the unbraced length has a negative impact on the capacity and stability of the piles. On the other hand, the stiffness contributions of concrete encasements around piles is typically ignored during pile bent design and in specifications and manuals, despite the stiffness of the concrete encasement having a positive contribution to pile capacity and stability.

The Iowa Department of Transportation (DOT) rating engineer is sometimes asked by field personnel to make quick decisions regarding pile capacity and stability when scour is identified around bridge pile bents. To help rating engineers provide timely, realistic estimations of pile capacity, Deng et al. (2018) developed a rapid assessment tool to quickly assess pile capacity, also taking into account both the unbraced pile lengths and the stiffness contribution of concrete encasements.

A numerical evaluation program was developed and implemented to offer a user-friendly assessment tool that could be used to quickly evaluate pile strength. The numerical program consisted of finite element (FE) models established for steel H-piles with or without concrete encasement and with consideration of linear and non-linear buckling and behavior.

The FE models were validated against capacities calculated based on the provisions outlined in the American Institute of Steel Construction (AISC) Steel Construction Manual (2017). After that, a parametric study was conducted to understand the influence of concrete encasements on pile buckling strength. Various combinations of the unbraced pile lengths and concrete encasement lengths were investigated. The relationships between buckling strength of the steel H-piles with concrete encasements under concentric and eccentric loading conditions were derived from the results of the parametric studies.

For the user's convenience, the researchers developed a graphical user interface for the tool, which requires the input of four parameters: loading eccentricity, H-pile section type, unbraced pile length, and concrete encasement length. This pile assessment tool can be utilized to quickly calculate pile capacity and assist state rating engineers in making rapid decisions regarding pile capacity. However, this rapid pile assessment tool was developed and verified using provisions and theoretical modeling approaches. Experimental data to validate the tool's results were not available or part of that study.

## **1.2 Objective**

The main objective of this research project was to validate the rapid pile assessment tool's findings to ensure accurate pile capacity determination, both for bare piles and those encased in concrete.

## **1.3 Report Content**

The remainder of this report includes four chapters followed by the References:

- Chapter 2. Literature Review
- Chapter 3. Laboratory Testing
- Chapter 4. Assessment Tool Validation
- Chapter 5. Summary and Conclusions

## CHAPTER 2. LITERATURE REVIEW

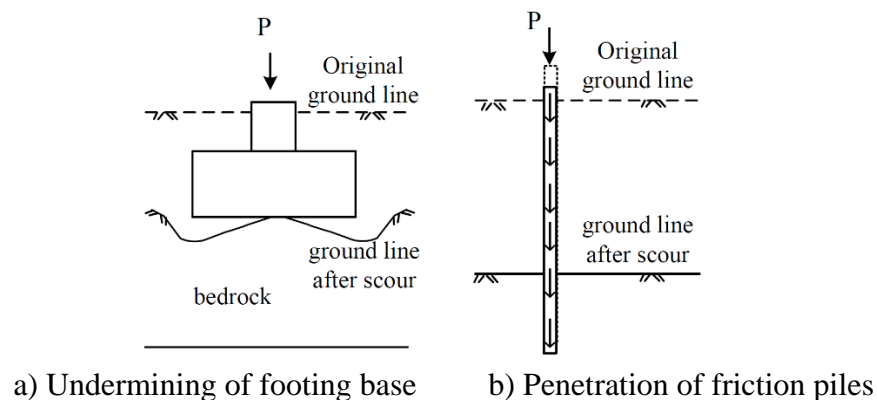
This chapter discusses scour as a primary phenomenon in reducing the capacity of bridge foundations and the effect of scour on pile foundations. This chapter also presents and discusses the concrete encasement details utilized by the Iowa DOT for piles.

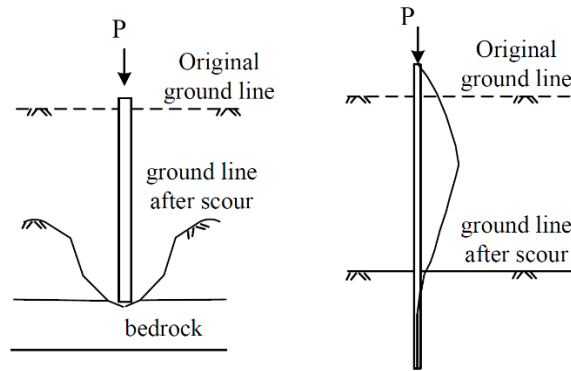
Scour is defined as “the erosion or removal of streambed or bank material from bridge foundations due to flowing water” (Kattell and Eriksson 1998). With this natural phenomenon, a flowing stream erodes the streambed gradually and without warning. Based on the investigation of more than 500 bridge failures in the US in 2003, Wardhana and Hadipriono (2003) found that more than 50% of bridge failures could be attributed to scour caused by floods and other hydraulic parameters. Lagasse et al. (2007) also reported that approximately 60% of bridge failures are caused by scour.

Scour is categorized into four main categories: general scour, channel migration, counteraction scour, and local scour. The occurrence of general scour is independent of the existence of the bridge, and it can occur as either long-term or short-term scour. With this phenomenon, the soil and other materials are removed from all or most of the width of the bed and bank of a channel (Fischenich and Landers 2000), while counteraction and local types of scour are related to the existence of the bridge (Liang et al. 2009).

Based on an investigation conducted by Lin et al. (2015) on 36 historical cases of bridge failure due to scour, local scour occurred in 64% of bridge failures, followed by channel migration (14%), and contraction scour (5%). Possible bridge failure modes due to scour included vertical failure, lateral failure, torsional failure, and bridge deck failure. Approximately 70% of bridge failures were lateral (39%) and vertical (30%) (Lin et al. 2014).

Lin et al. (2014) considered the combination of four main factors attributing to vertical failure of bridges under scour conditions. As illustrated in Figure 1, these factors include inadequate bearing capacity of soil (shallow foundations), penetration of friction piles, undermining of the pile toe, and pile buckling.





c) Undermining of pile tip      d) Buckling of piles  
Lin et al. 2014

### Figure 1. Vertical failure modes of bridge foundations

According to these factors, it can be concluded that the primary factors that determine the vulnerability of a bridge to scour damage is the type of foundation.

Based on research conducted by Kattell and Eriksson (1998), shallow foundations such as spread footings, short piles, mud sills, or cribs are considered highly vulnerable to scour. On the other hand, deep foundations such as long piles or drilled shafts are less vulnerable to scour damage and may be considered in a low risk category (Kattell and Eriksson 1998).

From a design viewpoint, foundations for new bridges should be designed with an accurate prediction of scour depths for design floods. Underestimation of scour depths may result in costly bridge repairs in the future or even catastrophic failures, while overestimation may cause costly and unnecessarily deep foundations.

The scour potential evaluation is also important for existing bridges. Overestimation of scour depths causes more bridges to be misclassified as “scour critical,” resulting in unnecessary installation of scour countermeasures or bridge replacements. In fact, some of those “scour-critical” bridges may be from scour overestimation due to improper use of assumptions or engineering judgments based on the inaccuracy of scour prediction equations (Zhang et al. 2013).

It is critical for state DOTs to quickly and effectively determine which bridges in their inventories are actually scour-critical, enabling responsible management of those bridges during and after scour events. Based on the Iowa DOT’s 2021 LRFD Bridge Design Manual, numerous factors affect the scour condition of bridges and need to be considered when designing new bridges or rehabilitating existing bridges.

One important factor is the substructure. Generally, it is suggested that wider and longer piers can cause greater scour. On the other hand, deeper footings and longer piles are more stable at greater scour depths. Spread footings should only be used with materials highly resistant to scour, such as limestone and some shale. It is also suggested that, in order to maintain the

integrity of the structure, scour is not to reduce pile bearings below a desirable safety factor per the structural or geotechnical engineer's judgment. Designing for this minimum safety factor sometimes requires designing longer piles for new bridges. However, for existing structures, protection of the piles may be necessary to maintain the safety factor determined as needed.

Previous research has been conducted regarding the buckling of piles under scour situations. Hughes et al. (2007a, b) showed that the elastic buckling capacity and stability of piles vary inversely with the square of the pile length. For example, in a scour of 15 ft at a pile bent with an original length of 15 ft, the elastic buckling capacity is reduced by a factor of 4.

The effects of a cross-bracing system on pushover capacity for extreme scour and flood events were also investigated. The results indicated that, for scour levels exceeding 5 ft, nearly all of the additional pushover capacity gained by adding cross-bracing is lost. The additional stiffness provided from the cross-bracing was lost more gradually as scour increased to approximately 15 ft. For this study, the researchers considered HP-10×42 pile sections without any concrete encasement.

Lin et al. (2012) investigated the effect of the superstructure in an integrated analysis of Kansas Bridge 45, considering the interaction between water, soil, pile foundation, and the bridge superstructure elements for scour conditions. The results of this research showed that scour increases the lateral deflections of pile caps exponentially.

Liang et al. (2015) investigated the stress history effect of remaining layered soft clay after scour. In their analytical model, the lateral subgrade modulus that was correlated to the undrained shear strength of soft clay was modified to account for the stress history effect after scour. The researchers concluded that extreme scour causes a significant change in the undrained shear strength of the remaining soils, and this change contributes to the difference in the pile buckling load when the stress history is considered or neglected. The results revealed that, when the scour depth is increased, the stress history effect could cause a 12% to 14% decrease in buckling load versus the results when ignoring the stress history effects.

The deterioration of piling systems caused by corrosion can cost \$1 billion annually for repair and replacement and can also endanger the safety and functionality of bridges (Lampo et al. 1998). The various methods to reduce the potential of deterioration of steel piles include protective coatings, cathodic protection, use of special steel alloys, and increasing the steel area and cast-in-place concrete encasements (AASHTO 2012). Concrete encasements are considered a non-structural element of the pile and their structural effect is usually neglected when piles are designed. Generally, in design codes like AASHTO's, there are no specific requirements for these encased sections.

In some states, the concrete encasement is not considered on the entire length of the exposed pile. With this method, only some specific length of the pile that is more prone to corrosion or the length that is already corroded is encased in the concrete, as shown in Figure 2.



Ainge 2012

**Figure 2. Steel H-pile concrete encasement for rehabilitation purposes used in Ohio**

However, the Iowa DOT uses continuous concrete encasement along the piles in square or circular cross-sections, as shown in Figure 3.



a) Circular encasements



b) Square encasements

**Figure 3. Steel H-piles with concrete encasement used in Iowa**

A specific standard for concrete encasements of steel H-piles was developed by the Iowa DOT, as shown in Figure 4.

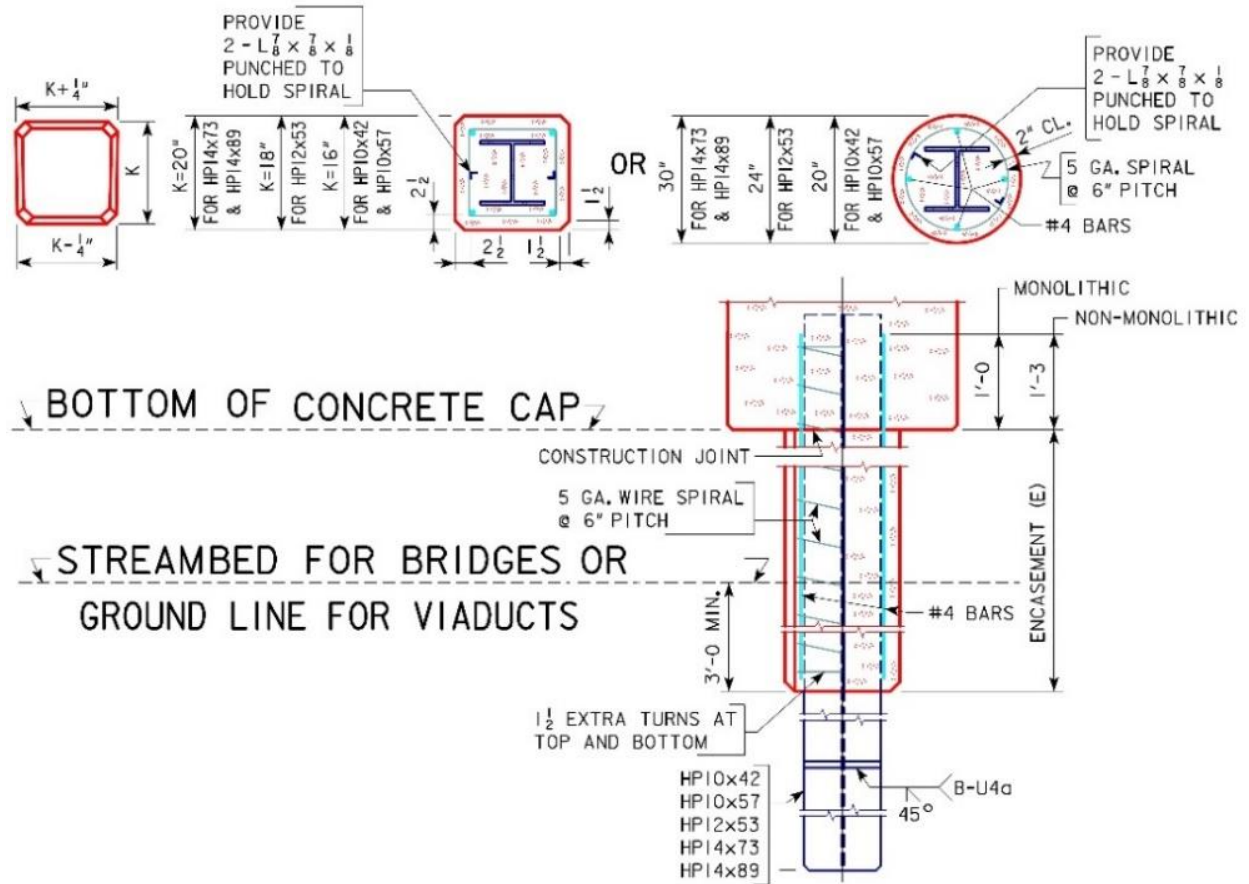


**Figure 4. Iowa DOT concrete encasement standard for H-piles**

Based on this standard, concrete encasement begins at the pile cap and extends at least 3 ft below the ground surface. The encasement can be a circular or square cross-section, and the dimension depends on the length of the pile above the ground.

## CHAPTER 3. LABORATORY TESTING

To provide sufficient data for the validation of the rapid assessment tool developed during the Phase I research, a series of experimental tests was conducted. Four specimens with different pile lengths and concrete encasement lengths and ratios were constructed and tested with concentric axial loading in the laboratory.

In this chapter, the test design, specimen construction, test setup, and instrumentation plan are presented in Section 3.1, 3.2, 3.3, and 3.4, respectively. The results from each test are presented and discussed in Section 3.5. The comparison of the results between the experimental tests and those from the assessment tool is provided in Chapter 4.

### 3.1 Test Design

Generally, the three main failure mechanisms for members under axial load fall under the categories of yielding, inelastic, and elastic buckling failures. For the yielding mechanism, which usually happens in short members, the axial stress reaches the yielding point in all depths of a specific cross-section before buckling happens. This type of failure is mostly dependent on the material characteristics of the member. Elastic buckling happens when the member loses its load-resisting capacity before the stress reaches the yielding point along the member length. This type of failure, which usually happens in long and slender members, is related to its structural properties. Inelastic buckling usually happens in members with medium slenderness. In this type of failure, the axial stress reaches the yielding strength in a portion of the cross-section while the remaining cross-section remains elastic.

With the intent to cover all three mechanisms discussed above, three different lengths of pile were chosen to represent short, medium, and long lengths. Laboratory tests were performed on four ASTM A572 Grade 50 HP10×42 steel pile sections, as summarized in Table 1.

**Table 1. Specimen details**

Specimen	Section	Pile length (ft)	Encasement length (ft)
1	HP10×42	16	N/A
2	HP10×42	16	10
3	HP10×42	30	20
4	HP10×42	38	30

The first and second specimens were 16 ft long, representing the short member. The third member had a medium length of 30 ft, and the fourth specimen was the longest specimen with a length of 38 ft. All members had concrete encasement except for the first specimen. The second, third, and fourth specimens had 10 ft, 20 ft, and 30 ft long concrete encasement, respectively. The details of the encasements were based on the Iowa DOT standard previously shown in Figure 4.

All four piles were tested with a fixed-pin support condition as assumed in the Phase I research (Deng et al. 2018) and loaded via concentric loading.

### 3.2 Specimen Construction

The specimens were constructed in the Structural Laboratory at Iowa State University. According to the P10L standard from the Iowa DOT, the square spirals with 6 in. pitch were placed around the piles. A steel plate was welded to the end of the pile to distribute the axial load evenly across the cross-section of each pile. After preparing the formwork for all three specimens, the concrete was poured for all of them at once. Figure 5 shows the prepared piles with concrete encasements for the third and fourth specimens.



**Figure 5. Specimen-3 and Specimen-4**

The compressive strength of the encasement concrete was tested at the date that each of Specimen-2 to Specimen-4 was tested. Table 2 shows the test dates and the strengths of the concrete samples for encasement.

**Table 2. Material properties**

Sample	Pour date	Test date	Compressive strength (psi)	Average compressive strength (psi)
1	08/10/2020	10/19/2020	6,380	6,345
2	08/10/2020	10/19/2020	6,309	
3	08/10/2020	01/20/2021	6,451	6,653
4	08/10/2020	01/20/2021	6,855	
5	08/10/2020	05/10/2021	7,115	7,090
6	08/10/2020	05/10/2021	7,066	

In total, six 4×4 in. cylinders were tested according to ASTM C39 (2018). The results showed growing strength of the concrete as its age increased, as would be expected.

### 3.3 Test Setup and Loading Configuration

To evaluate the axial capacity of the piles, an axial load needed to be applied to the pile ends. Given that the longest pile length was 38 ft, and it was not possible to test this specimen length vertically, the test setup was designed in a way that the piles could be tested in a horizontal direction while still achieving axial loading. The challenge with the horizontal testing was to provide structural support at both ends of each pile.

The results of the numerical simulations in the first phase of this research revealed that a large axial load of about 600 kips was needed to make a 16 ft long encased H10×42 pile buckle. This axial load needs reasonable supports to transfer the load to the ground by friction forces. As a result, to provide adequate friction forces between the floor and supports, large concrete blocks were constructed. Figure 6 shows the schematic view of this test setup for all specimens.

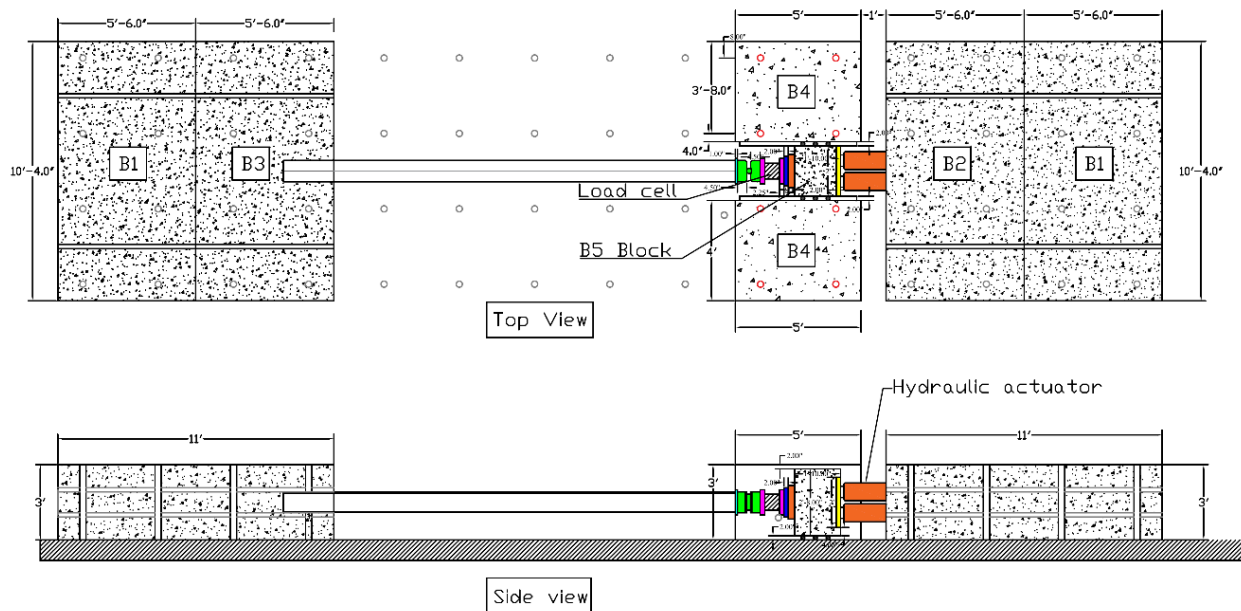


**Figure 6. Test setup**

The maximum capacity of the available crane in the laboratory was a limiting factor; thus, the concrete blocks at each side of each pile were built in two smaller blocks (B1, B2, and B3) and then post-tensioned in the horizontal direction. Finally, all the concrete blocks on both sides were post-tensioned to the laboratory floor to add enough vertical load to result in more friction counteracting forces.

In this setup, four hydraulic actuators (Figure 7-a), with 200 kips capacity on each, were mounted horizontally on the support concrete block to apply the axial load to the pile pin-end.



a) Hydraulic actuators.



b) B5 block and two B4 blocks and side rollers.

**Figure 7. Pile pin-end setup**

To combine the force from all actuators, a small concrete block (block B5 in the previous Figure 6) was constructed and positioned between the two side blocks (block B4 in Figure 6). The B4 blocks were used to prevent the B5 block from moving in the transverse direction. Rollers were used between the B5 block and to the B4 side blocks to ease the movement of the B5 block in the axial direction. Figure 7-b shows the test setup for the pile pin end with the B5 block and two B4 blocks.

To achieve a pin-end condition at the end of the pile, two thick plates with a dimension of 10×10×4.5 in. were used. On one of these plates, a cylindrical concaved shape was constructed, and a corresponding cylindrical part was welded to the other plate. Figure 8 shows the pin connection at the end of the pile.



a) Cylindrical concaved shape



b) Cylindrical part



c) Pin connection

**Figure 8. Pin connection details**

The other end of the pile, which is assumed to be in the soil, was constructed with a fixed-end condition. The fixity was achieved by embedding 2 ft of pile into the concrete block. Previous studies confirmed that this length of embedment can provide complete fixity at the end of the

member (Castilla et al. 1984). Figure 9-a shows the pile embedment inside the concrete block before pouring the concrete.



a) Reinforcement arrangement in the concrete block B3

b) Fixed end



c) Pin support end

**Figure 9. Pile fixity inside the concrete block**

Hoops were used around the pile inside the block to apply more confinement to the concrete around the pile and increase the shear strength. Figure 9-b and -c show the test setup at the fixed and pin end, respectively.

### **3.4 Instrumentation Plans**

During the tests, three types of measurements were obtained via strain gauges, load cells, and displacement transducers. The load cell recorded the axial load reached at the pin end of the pile. The deformation of the piles was measured using the transducers, and the strain values on the steel or concrete encasement surfaces at critical locations were measured using the strain gauges.

In general, 15 to 20 strain gauges and 10 to 14 displacement transducers were used for each specimen. Data were observed and collected during the experiments and exported and post-

processed using MATLAB. The positions of the sensors for each specimen are presented in the following sections in more detail.

### 3.4.1 Specimen-1 Instrumentation Plan

Specimen-1 was 16 ft long without any concrete encasement. The instrumentation plan for Specimen-1 is shown in Figure 10.

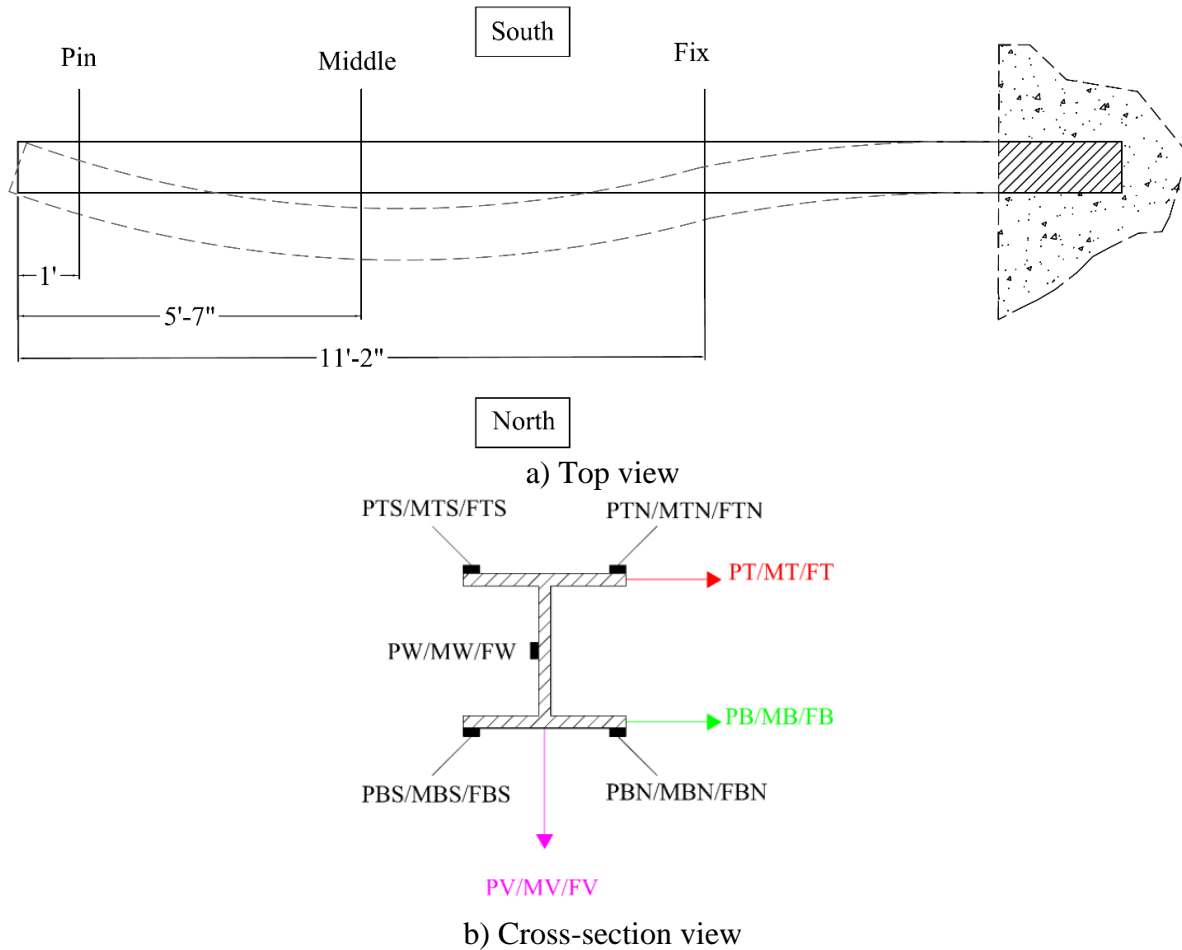


**Figure 10. Instrumentation on Specimen-1**

The gauges were installed in three instrumentation sections labeled as pin (P), middle (M), and fix (F). The P section was 1 ft from the pinned end of the pile. The M section was 5 ft 7 in. from the pinned end (0.35L). The F section was close to the fixed end of the pile and was 11 ft 2 in. from the pinned end (0.7L)

The strain gauges were installed to measure the axial strain of the pile on both the north and south sides of the pile. The labels N and S designate those sides of the pile, respectively, and T, B, and M designate the top flange, bottom flange, and middle or web, respectively. In each instrumentation section, five strain gauges were installed with two on the top flange, two on the

bottom flange, and one in the middle of the web. The strain gauges on the top and bottom flanges were installed 0.5 in. from the edges of the flanges.

Displacement transducers were utilized to measure the deformation of the specimen during the test. The axial displacement of the pile was recorded with a displacement transducer called PA at the P section. To check if the pile experienced any torsional behavior during buckling, displacement transducers were placed on the top and bottom edges. In addition, one transducer was placed in each instrumentation section to measure vertical displacement. Table 3 presents the label and position for each gauge installed on Specimen-1.

**Table 3. Instrumentation details for Specimen-1**

#	Label	Type	Instrumentation section	Position in section	Distance from pinned end
1	PTN	SG	Pin	Top flange	1 ft
2	PTS	SG	Pin	Top flange	1 ft
3	PBN	SG	Pin	Bottom flange	1 ft
4	PBS	SG	Pin	Bottom flange	1 ft
5	PW	SG	Pin	Web	1 ft
6	MTN	SG	Middle	Top flange	5 ft 7 in.
7	MTS	SG	Middle	Top flange	5 ft 7 in.
8	MBN	SG	Middle	Bottom flange	5 ft 7 in.
9	MBS	SG	Middle	Bottom flange	5 ft 7 in.
10	MW	SG	Middle	Web	5 ft 7 in.
11	FTN	SG	Fix	Top flange	11 ft 2 in.
12	FTS	SG	Fix	Top flange	11 ft 2 in.
13	FBN	SG	Fix	Bottom flange	11 ft 2 in.
14	FBS	SG	Fix	Bottom flange	11 ft 2 in.
15	FW	SG	Fix	Web	11 ft 2 in.
16	PT	DT	Pinned end	Top flange	2 in.
17	PB	DT	Pinned end	Top flange	2 in.
18	PV	DT	Pinned end	Bottom flange	2 in.
19	PA	DT	Pinned end	Top flange	0
20	MT	DT	Middle	Top flange	5 ft 7 in.
21	MB	DT	Middle	Bottom flange	5 ft 7 in.
22	MV	DT	Middle	Bottom flange	5 ft 7 in.
23	FT	DT	Fix	Top flange	11 ft 2 in.
24	FB	DT	Fix	Bottom flange	11 ft 2 in.
25	FV	DT	Fix	Bottom flange	11 ft 2 in.

SG = strain gauge, DT = displacement transducer

### 3.4.2 Specimen-2 Instrumentation Plan

Specimen-2 was 16 ft long and had a 10 ft long concrete encasement. For this specimen, the data were recorded in four main instrumentation sections named pin (P), concrete (C), middle (M), and fix (F), as shown in Figure 11-a.

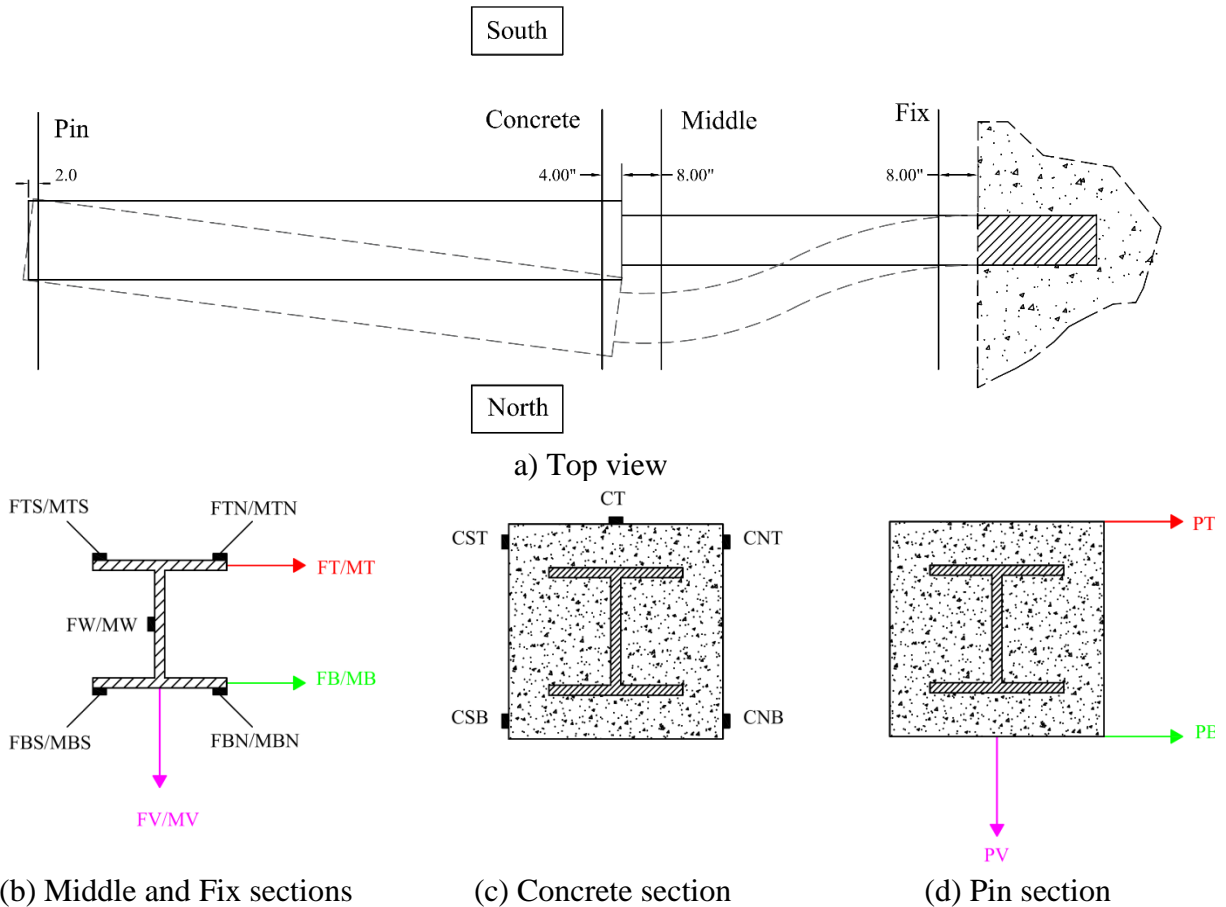


**Figure 11. Instrumentation on Specimen-2**

The P section was 2 in. from the pin end of the pile. The C section was 4 in. from the end of the concrete encasement, and the M section was 8 in. from the end of the concrete encasement. The F section was 8 in. from the concrete block at the fixed end of the pile.

Similar to Specimen-1, strain gauges were installed on the north and south sides of the pile, as shown in Figure 11-b, -c, and -d, and labeled in the same way as those for Specimen-1. Displacement transducers were installed in the P, M, and F sections. In these sections, two transducers recorded displacements in the transverse direction, and one measured vertical displacement, as illustrated in Figure 11-b and -d. The axial displacement of the pile along its longitudinal direction was also recorded in the P section. Table 4 provides detailed information for each strain gauge and displacement transducer on Specimen-2.

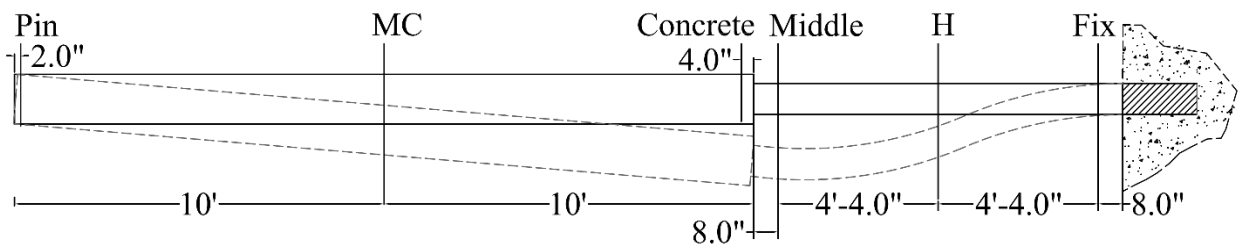
**Table 4. Instrumentation details for Specimen-2**

#	Label	Type	Instrumentation section	Position in section	Distance from pinned end
1	CST	SG	Concrete	Top edge	9 ft 8 in.
2	CNT	SG	Concrete	Top edge	9 ft 8 in.
3	CSB	SG	Concrete	Bottom edge	9 ft 8 in.
4	CNB	SG	Concrete	Bottom edge	9 ft 8 in.
5	CT	SG	Concrete	Top surface	9 ft 8 in.
6	MTN	SG	Middle	Top flange	10 ft 8 in.
7	MTS	SG	Middle	Top flange	10 ft 8 in.
8	MBN	SG	Middle	Bottom flange	10 ft 8 in.
9	MBS	SG	Middle	Bottom flange	10 ft 8 in.
10	MW	SG	Middle	Web	10 ft 8 in.
11	FTN	SG	Fix	Top flange	15 ft 4 in.
12	FTS	SG	Fix	Top flange	15 ft 4 in.
13	FBN	SG	Fix	Bottom flange	15 ft 4 in.
14	FBS	SG	Fix	Bottom flange	15 ft 4 in.
15	FW	SG	Fix	Web	15 ft 4 in.
16	PT	DT	Pin	Top edge	2 in.
17	PB	DT	Pin	Bottom edge	2 in.
18	PV	DT	Pin	Bottom surface	2 in.
19	PA	DT	Pin	Top edge	0
20	MT	DT	Middle	Top flange	10 ft 8 in.
21	MB	DT	Middle	Bottom flange	10 ft 8 in.
22	MV	DT	Middle	Bottom flange	10 ft 8 in.
23	FT	DT	Fix	Top flange	15 ft 4 in.
24	FB	DT	Fix	Bottom flange	15 ft 4 in.
25	PT	DT	Pin	Top edge	2 in.

SG = strain gauge, DT = displacement transducer

### 3.4.3 Specimen-3 Instrumentation Plan

Specimen-3 was 30 ft long with a 20 ft long concrete encasement. The instrumentation plan for Specimen-3 is shown in Figure 12.



a) Top view

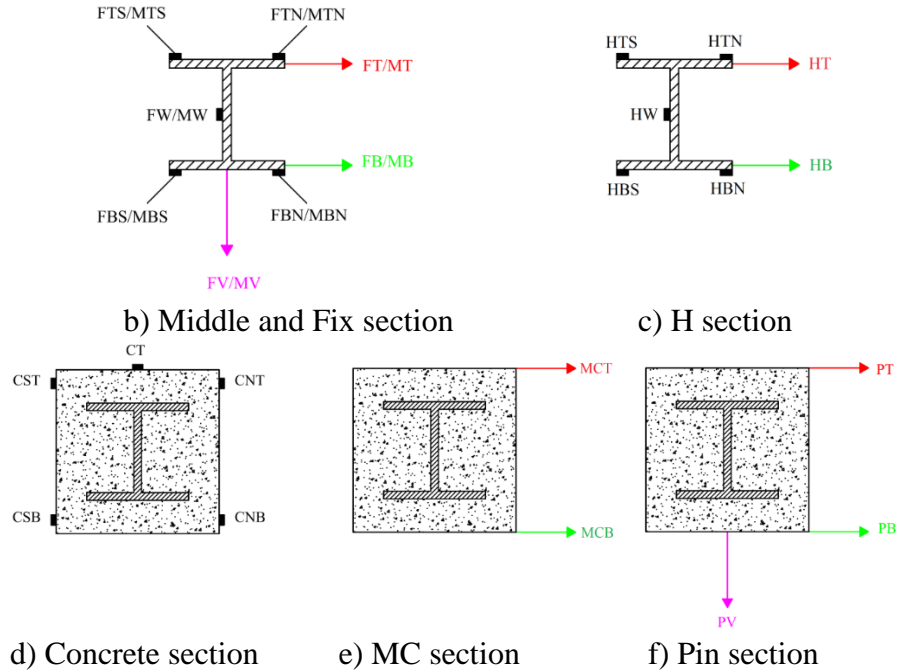


**Figure 12. Instrumentation on Specimen-3**

Similar to Specimen-2, data were recorded in sections P, C, M, and F. However, given that the pile and concrete encasement were longer than those for Specimen-2, two additional sections were evaluated along the pile: one in the middle of the concrete encasement, labeled MC in Figure 12-a, and the other in the middle of the steel section, labeled H.

Strain gauges and displacement transducers were installed and labeled in the same way as those for Specimen-2. Figure 12-b through -f show the details for each instrumentation section. Table 5 presents the detailed information for all of the instrumentation on Specimen-3.

**Table 5. Instrumentation details for Specimen-3**

#	Label	Type	Instrumentation section	Position in section	Distance from pinned end
1	CST	SG	Concrete	Top edge	19 ft 8 in.
2	CNT	SG	Concrete	Top edge	19 ft 8 in.
3	CSB	SG	Concrete	Bottom edge	19 ft 8 in.
4	CNB	SG	Concrete	Bottom edge	19 ft 8 in.
5	CT	SG	Concrete	Top surface	19 ft 8 in.
6	MTN	SG	Middle	Top flange	20 ft 8 in.
7	MTS	SG	Middle	Top flange	20 ft 8 in.
8	MBN	SG	Middle	Bottom flange	20 ft 8 in.
9	MBS	SG	Middle	Bottom flange	20 ft 8 in.
10	MW	SG	Middle	Web	20 ft 8 in.
11	HTN	SG	H	Top flange	25 ft
12	HTS	SG	H	Top flange	25 ft
13	HBN	SG	H	Bottom flange	25 ft
14	HBS	SG	H	Bottom flange	25 ft
15	HW	SG	H	Web	25 ft
16	FTN	SG	Fix	Top flange	29 ft 4 in.
17	FTS	SG	Fix	Top flange	29 ft 4 in.
18	FBN	SG	Fix	Bottom flange	29 ft 4 in.
19	FBS	SG	Fix	Bottom flange	29 ft 4 in.
20	FW	SG	Fix	Web	29 ft 4 in.
21	PT	DT	Pin	Top edge	2 in.
22	PB	DT	Pin	Bottom edge	2 in.
23	PV	DT	Pin	Bottom surface	2 in.
24	PA	DT	Pin	Top edge	0
25	MCT	DT	MC	Top edge	10 ft
26	MCB	DT	MC	Bottom edge	10 ft
27	MT	DT	Middle	Top flange	20 ft 8 in.
28	MB	DT	Middle	Bottom flange	20 ft 8 in.
29	MV	DT	Middle	Bottom flange	20 ft 8 in.
30	HT	DT	H	Top flange	25 ft
31	HB	DT	H	Bottom flange	25 ft
32	FT	DT	Fix	Top flange	29 ft 4 in.
33	FB	DT	Fix	Bottom flange	29 ft 4 in.
34	FV	DT	Fix	Bottom flange	29 ft 4 in.

SG = strain gauge, DT = displacement transducer

#### 3.4.4 Specimen-4 Instrumentation Plan

Specimen-4 was 38 ft long with a 30 ft long concrete encasement. The instrumentation plan for Specimen-4 is shown in Figure 13.

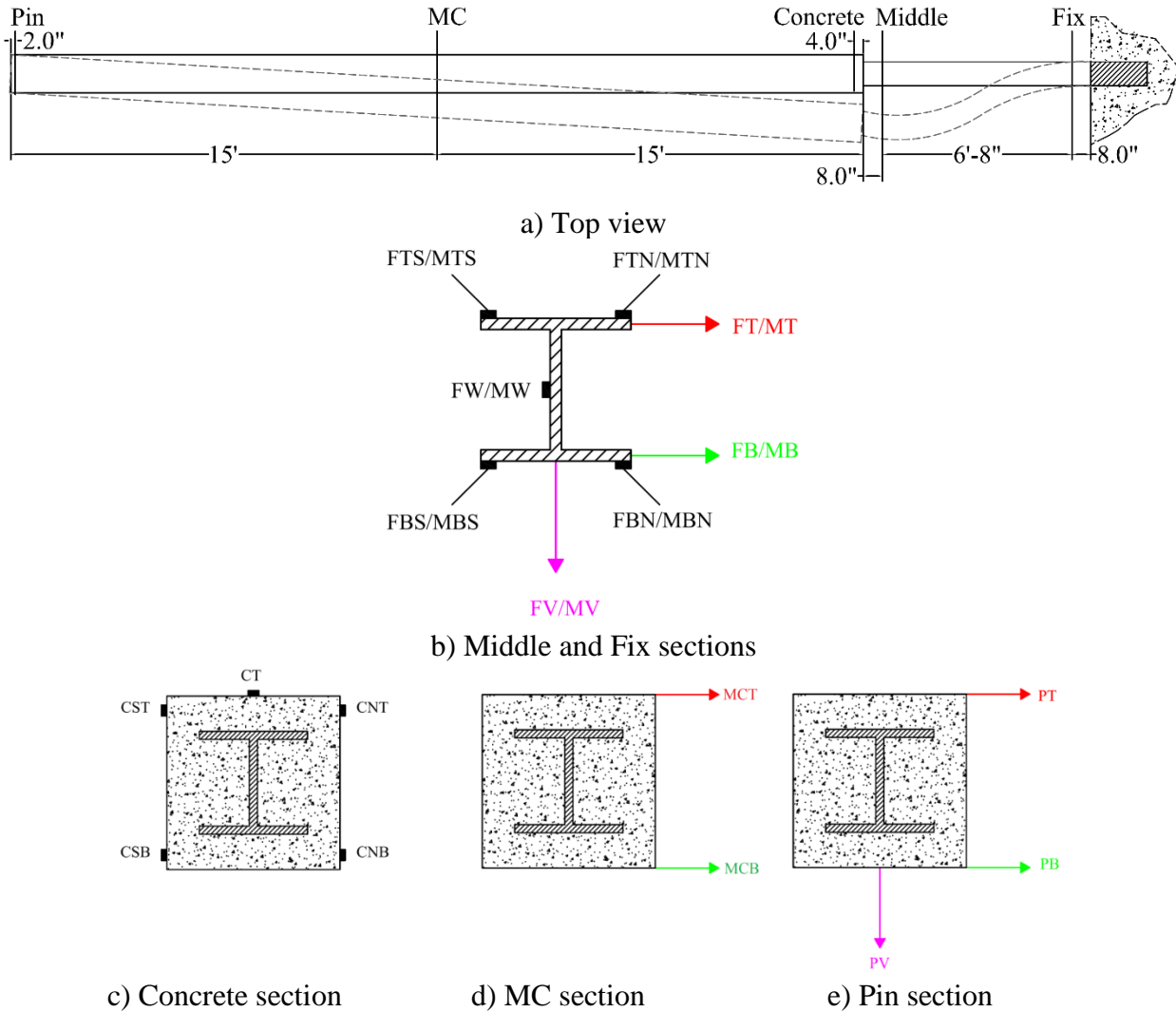


**Figure 13. Instrumentation on Specimen-4**

Similar to the other specimens, data were recorded in the P, C, M, and F sections (Figure 13-a). Also, in order to detect probable bending in the middle of the concrete encased section, similar to the Specimen-3, one additional section was evaluated in the middle of the concrete encasement, called MC. Strain gauges and displacement transducers were installed and labeled in the same way as with Specimen-3. Figure 13-b through -e show the details for each instrumentation section. Table 6 presents the detailed information for all of the measurements obtained from Specimen-4.

**Table 6. Instrumentation details from Specimen-4**

#	Label	Type	Instrumentation section	Position in section	Distance from pinned end
1	CST	SG	Concrete	Top edge	29 ft 8 in.
2	CNT	SG	Concrete	Top edge	29 ft 8 in.
3	CSB	SG	Concrete	Bottom edge	29 ft 8 in.
4	CNB	SG	Concrete	Bottom edge	29 ft 8 in.
5	CT	SG	Concrete	Top surface	29 ft 8 in.
6	MTN	SG	Middle	Top flange	30 ft 8 in.
7	MTS	SG	Middle	Top flange	30 ft 8 in.
8	MBN	SG	Middle	Bottom flange	30 ft 8 in.
9	MBS	SG	Middle	Bottom flange	30 ft 8 in.
10	MW	SG	Middle	Web	30 ft 8 in.
11	FTN	SG	Fix	Top flange	37 ft 4 in.
12	FTS	SG	Fix	Top flange	37 ft 4
13	FBN	SG	Fix	Bottom flange	37 ft 4
14	FBS	SG	Fix	Bottom flange	37 ft 4
15	FW	SG	Fix	Web	37 ft 4
16	PT	DT	Pin	Top edge	2 in.
17	PB	DT	Pin	Bottom edge	2 in.
18	PV	DT	Pin	Bottom surface	2 in.
19	PA	DT	Pin	Top edge	0
20	MCT	DT	MC	Top edge	15 ft
21	MCB	DT	MC	Bottom edge	15 ft
22	MT	DT	Middle	Top flange	30 ft 8 in.
23	MB	DT	Middle	Bottom flange	30 ft 8 in.
24	MV	DT	Middle	Bottom flange	30 ft 8 in.
25	FT	DT	Fix	Top flange	37 ft 4 in.
26	FB	DT	Fix	Bottom flange	37 ft 4 in.
27	FV	DT	Fix	Bottom flange	37 ft 4 in.

SG = strain gauge, DT = displacement transducer

### 3.4.5 Additional Instrumentation

One of the challenges in these tests was providing enough friction between the concrete blocks (B1, B2, and B3) and the ground to resist the horizontal load applied to the ends of the piles. To detect any movement of the blocks during testing, additional instrumentation was implemented. Two displacement transducers were mounted to each concrete block to measure any potential movement of the block in the horizontal or vertical direction, as shown Figure 14-a.



a) Transducers to check the movement of the blocks during the test



b) Transducers to check the fixity at the end of the piles

#### **Figure 14. Additional instrumentation**

These transducers were labeled WVB and WHB for the concrete block on the fixed end in the vertical and horizontal directions, respectively. For the pinned end of the piles, the transducers were labeled EVB and EHB for the vertical and horizontal directions, respectively. In addition, to check any potential sliding of the steel pile inside the concrete block, two displacement transducers, labeled PN and PS, were mounted on the fixed end of the pile. Those transducers were connected on the top of the top flange, as shown in Figure 14-b. The test results showed no significant relative displacement between the pile and the block, and the movement of the block was zero.

### 3.5 Test Results

This section presents and discusses the results for Specimen-1 through -4 in Section 3.5.1 through 3.5.4, respectively. A comprehensive comparison between the results for each specimen is included as Section 3.5.5.

#### 3.5.1 Specimen-1 Test Results

Specimen-1 was 16 ft long with no concrete encasement. Figure 15-a shows the deformed shape of the member after the global buckling occurred.



a) Buckling of Specimen-1



b) Local failure on flange (top)

c) Local failure on flange (side)

**Figure 15. Deformed shape of Specimen-1**

The pile reached its maximum axial capacity and experienced bending toward the north side along its weak axis. The maximum displacement occurred at the middle section (5 ft 7 in. from the pin end). Figure 15-b and -c show the deformation of the failure on both the top and bottom flanges at the M section. Before the load application, the specimen was painted white; the black color shown on the steel indicates significant strain occurring during the load application. Figure 16 shows the axial load-displacement curve.

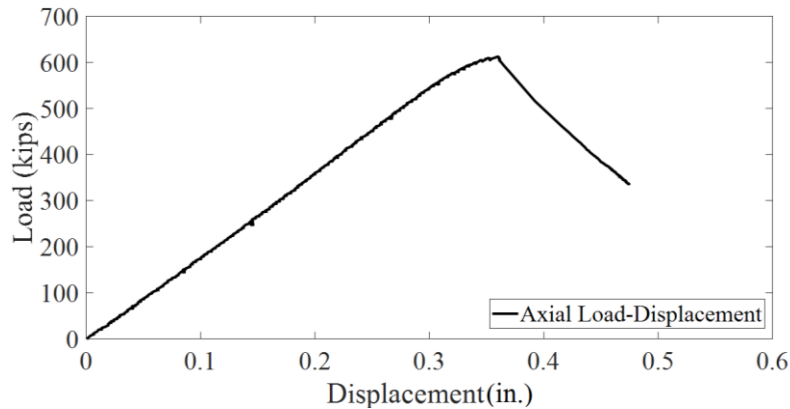
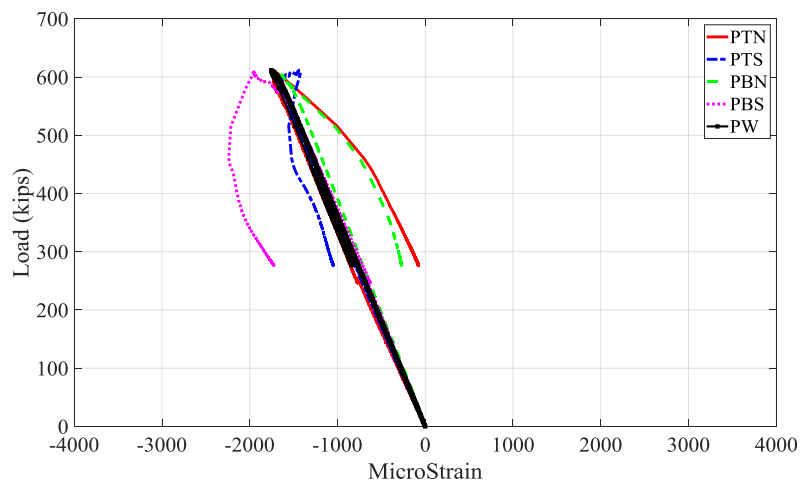


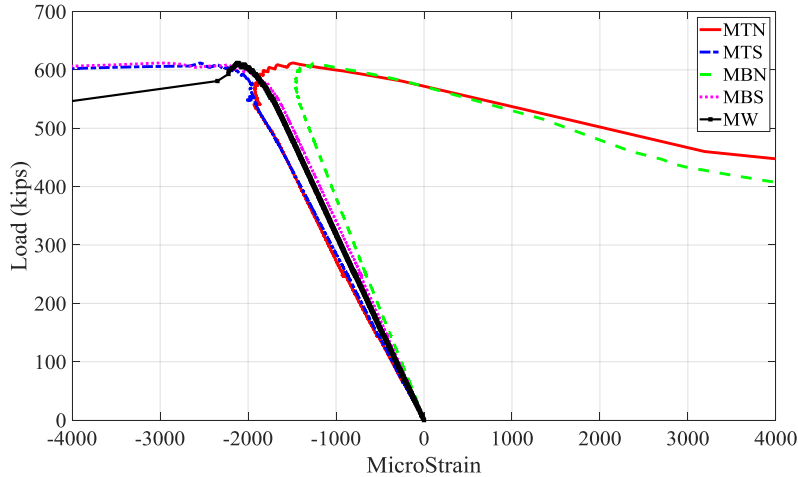
**Figure 16. Axial load-displacement of Specimen-1**

As the load increased, the axial displacement increased linearly until it reached 612.25 kips. At this point, the pile experienced an axial displacement of 0.4031 in. Beyond this point, the pile suddenly buckled, and the load-resisting capacity was lost. Assuming the yield strength of the pile steel is exactly 50 ksi, the yield strength of the full cross-section (with an area of 12.4 in.<sup>2</sup>) will be about 620 kips. This indicated that the Specimen-1 buckled right before the yielding of the full cross-section.

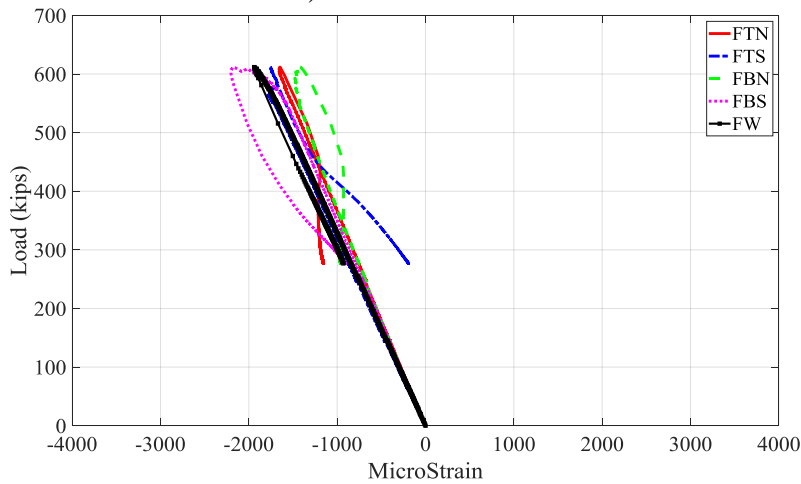
Figure 17-a shows the strain results collected from Section P (2 ft from the pinned end).



**a) Pin section**



b) Middle section



c) Fix section

**Figure 17. Strain data from Specimen-1**

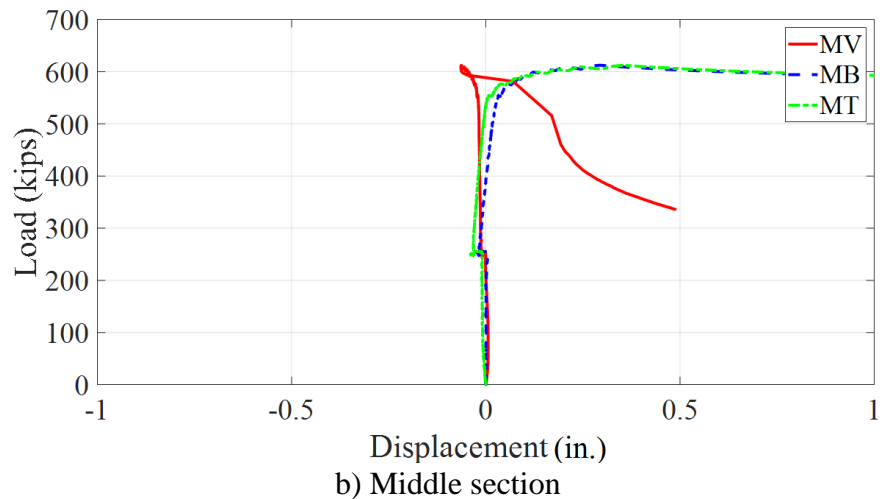
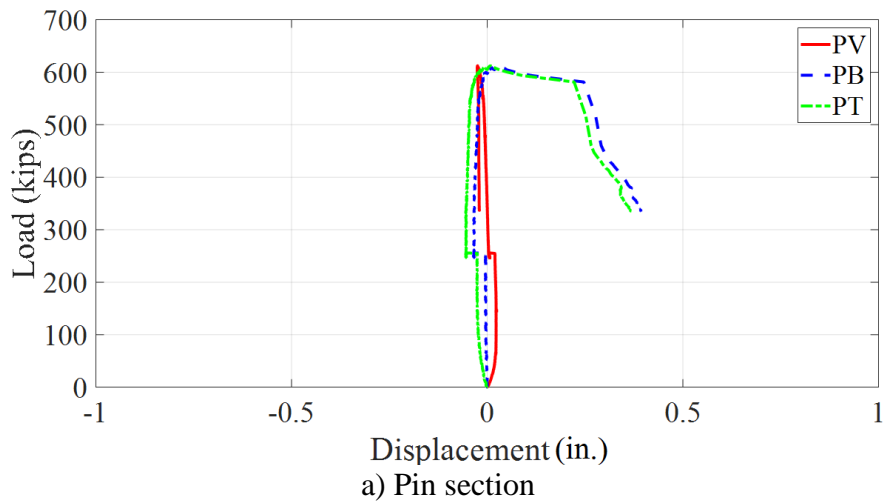
According to this diagram, the strain values increase linearly while the axial load increased. Except for PBS, other strain values in this section remained less than the yielding strain of about 0.0021 (2,100 microstrain), and the specimen remained in the elastic region. Since the deflection of the pile was toward the north side, this made the flanges on the north side experience tensile strain and the flanges on the south side experience compressive strain. After buckling, the compressive strain values in PTN and PBN decreased, while the strain in PTS and PBS increased and experienced more compressive strain. Based on Figure 17-a, the strain in the web (PW) decreased linearly after buckling occurred.

Figure 17-b shows the strain value in section M (5 ft 7 in. from the pinned end). According to this chart, the strain values increased linearly while the axial load increased. When the load reached the critical buckling point, all strain values in this section suddenly increased and passed the 0.0021 yielding strain limit. This shows that the specimen entered its plastic region in this section. Similar to the pin section, bending of the pile toward the north side made the flanges on this side experience tensile strain and the south flanges experience more compressive strain.

After buckling, the compressive strain values in MTN and MBN decreased, while MTS and MBS experienced more compressive strain.

Figure 17-c shows the strain in section F (11 ft 2 in. from the pinned end). The strain values increased linearly while the axial load increased. Similar to the pin section, except for FBS, other strain values in this section remained less than the yielding strain of about 0.0021 (2,100 microstrain), and the specimen remained in elastic region.

Figure 18 shows the axial load versus transverse and vertical displacement of the pile in sections P, M, and F.



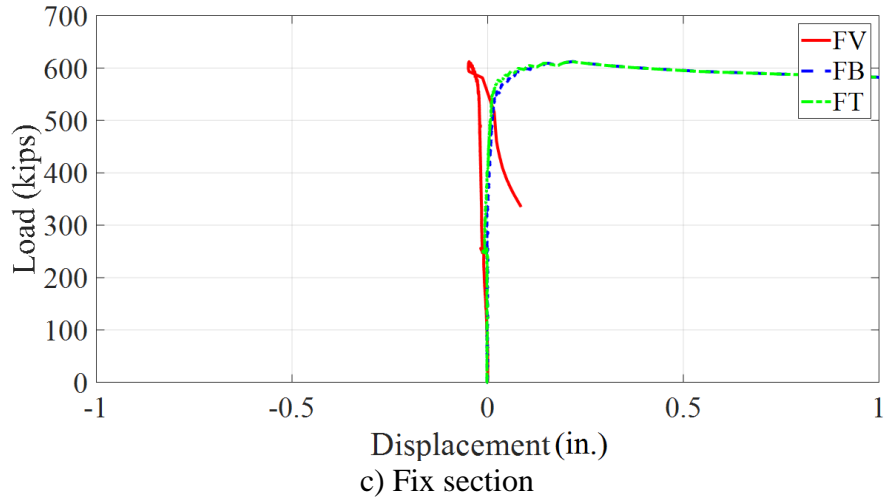
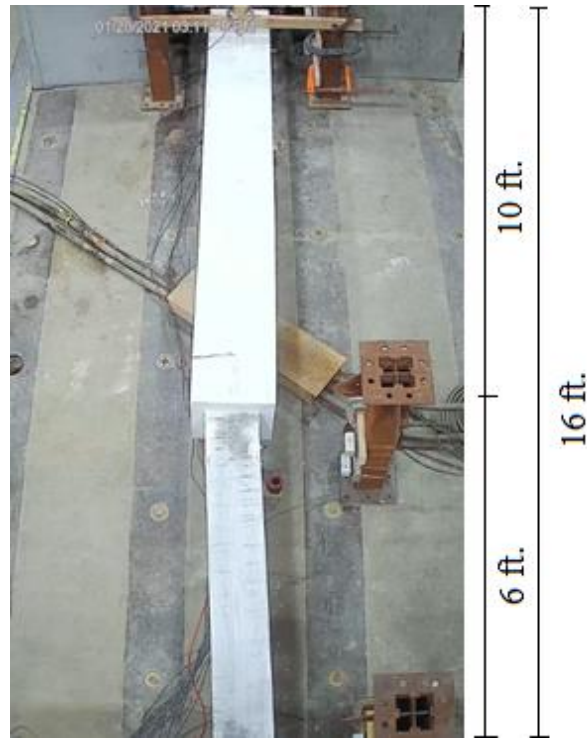


**Figure 18. Displacement data from Specimen-1**

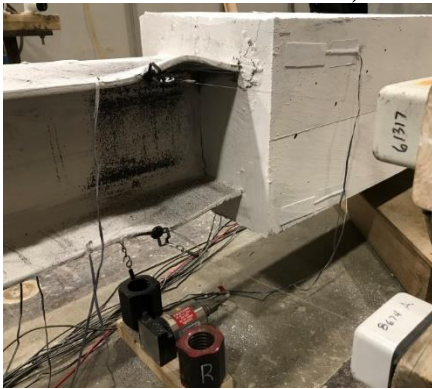
As the load increased, there was almost no significant transverse or vertical displacement prior to the buckling point. When the load approached the maximum, the transverse displacement gradually increased, and when the load reached its maximum value, buckling occurred and transverse displacement rapidly increased. Given that the transverse displacement on the top and bottom flanges (MT and MB) were similar, the pile did not experience significant torsion.

### 3.5.2 Specimen-2 Test Results

Specimen-2 was 16 ft long with a 10 ft long concrete encasement. Figure 19-a shows the deformed shape of this specimen after global buckling occurred.



a) Buckling of Specimen-2



b) Middle section (1)



c) Middle section (2)



d) Fix section (1)



e) Fix section (2)

**Figure 19. Deformed shape of Specimen-2**

The pile bent toward the north side about its weak axis. The maximum displacement occurred at section M (10 ft 8 in. from the pinned end). Figure 19-c through -e show the deformation in the M and F sections, respectively. The results indicated that the top and bottom flanges in both sections F and M experienced significant strain. This indicated that the plasticity occurred in both sections F and M.

Buckling also caused longitudinal and transverse cracks in the encasement. As shown in Figure 20, longitudinal cracking occurred along the pile, and transverse cracks occurred on all sides of the concrete encasement perpendicular to the pile axis.



**Figure 20. Crack pattern in the concrete encasement of Specimen-2**

Figure 21 shows the axial load-displacement curve for Specimen-2.

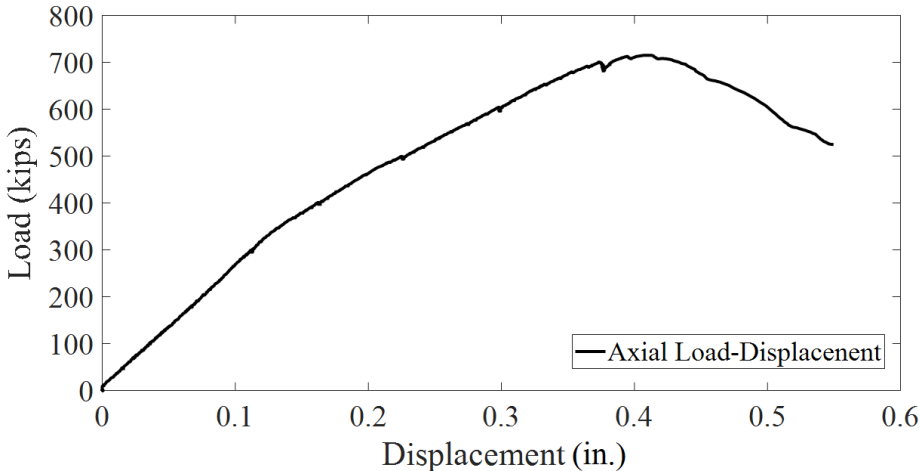


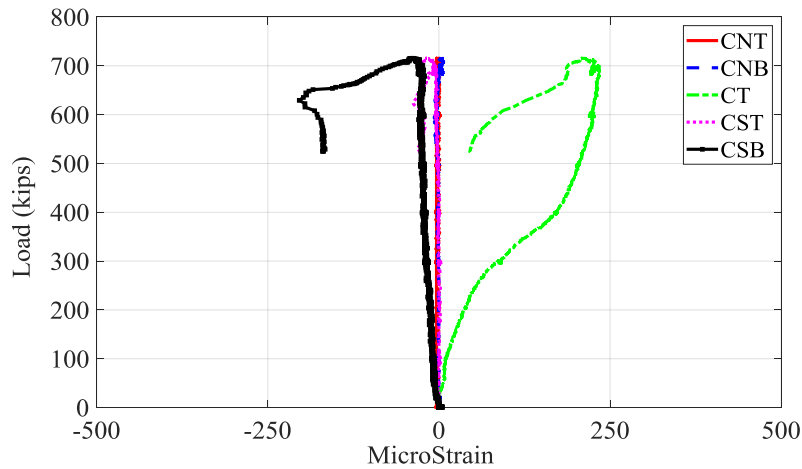
**Figure 21. Axial load-displacement of Specimen-2**

As the load increased, the axial displacement increased until it reached the critical load of 715 kips, which is about 103 kips higher than Specimen-1. At this point, the pile experienced 0.4087 in. axial displacement, which is similar to the axial displacement at buckling for Specimen-1

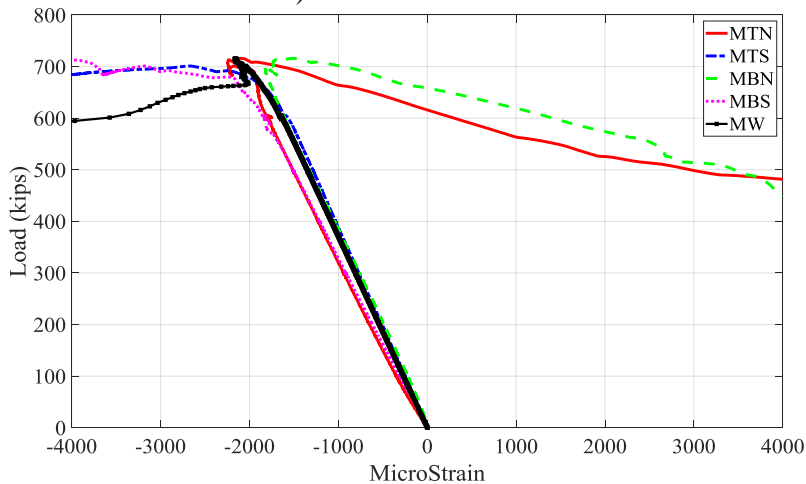
(0.4031 in.). After that, the pile suddenly buckled, and the load-resisting capacity was lost. The results indicated that the maximum capacity of Specimen-2 exceeds the full cross-section yield strength (620 kips) with an assumption of martial yield strength of 50 ksi. This reveals that the material ultimate strength is much higher than the yield strength. Salmon and Johnson (1996) indicated that the ultimate strength of Grade 50 steel could be up to 65–80 ksi.

Unlike Specimen-1 (as shown in the previous Figure 16), the load displacement curve for Specimen-2 was not perfectly linear prior to the critical load. The slope of the axial load-displacement curve changed when loading reached about 350 kips. This is because cracking occurred in the concrete encasement and reduced the cross-sectional stiffness.

Figure 22-a shows the strain data collected from the concrete section (4 in. from the end of the concrete encasement).



a) Concrete section



b) Middle section

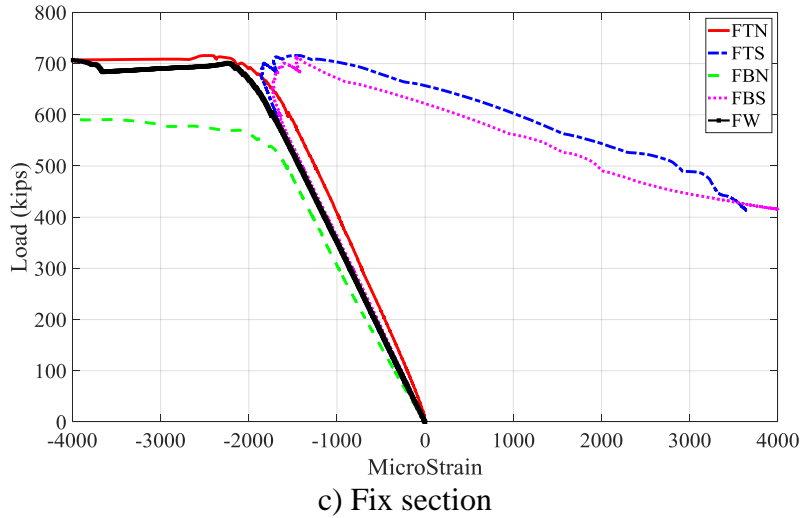
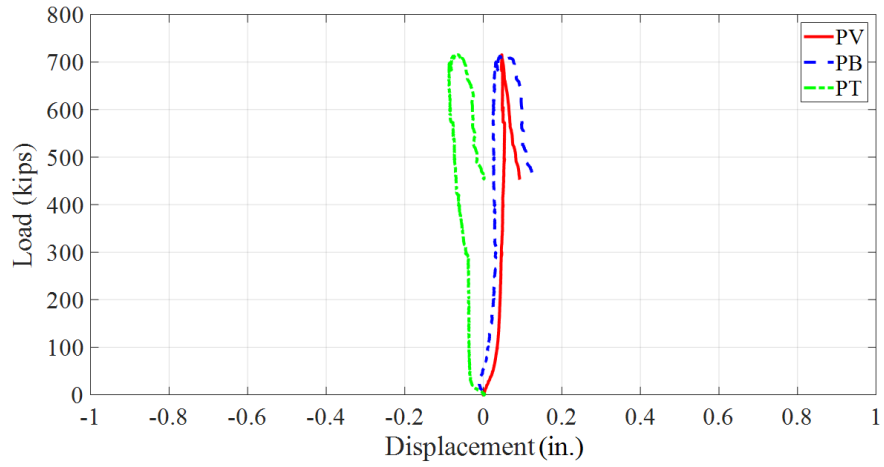


**Figure 22. Strain data from Specimen-2**

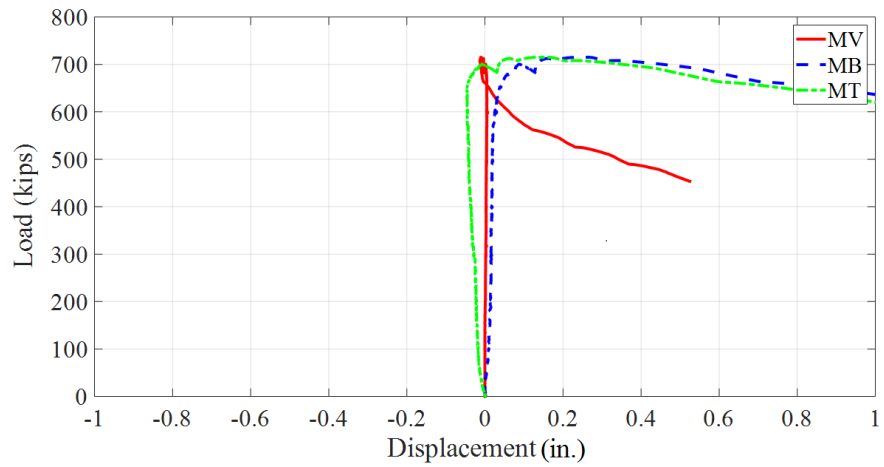
The results indicated that, except for CT, the strain values increased linearly with the axial load. The results also indicated that a tensile crack occurred near the CT strain gauge when the load reached 320 kips. The other strain gauges recorded compressive strain values in this section, and their values remained less than the ultimate compression strain of the concrete, which is considered as 0.003 based on ACI-318 code.

Figure 22-b shows the strain in the middle section (10 ft 8 in. from the pinned end of the pile). According to this chart, the strain values increased linearly while the axial load increased. When the load reached the critical buckling point, all strain values in this section suddenly increased and passed the 0.0021 yielding strain limit. This indicated that the specimen entered its plastic region in this section. Given that the pile buckled toward the north side, the flanges on the north side experienced tensile strain, and the south flanges experienced compressive strains. After buckling, strain values in MTN and MBN increased, which resulted in a reduction in compressive strain and eventually positive values. The strain values in MTS and MBS further decreased and experienced more compressive strain after buckling occurred. Figure 22-c shows the strain in section F (15 ft 4 in. from the pinned end). After the load reached the critical buckling point, the compressive strain on the north side further increased and the strains on the south side started to decrease. This stress change was the opposite of that for section M.

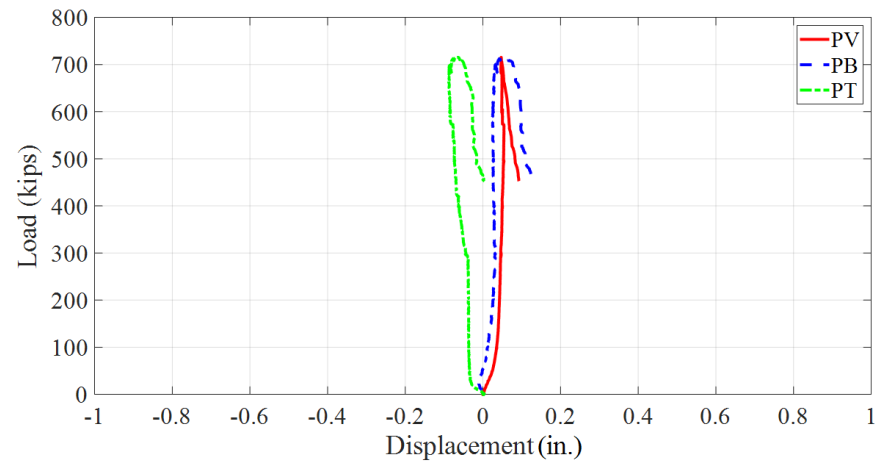
Figure 23 shows the axial load versus transverse and vertical displacement of the pile in sections P, M, and F.



a) Pin section



b) Middle section



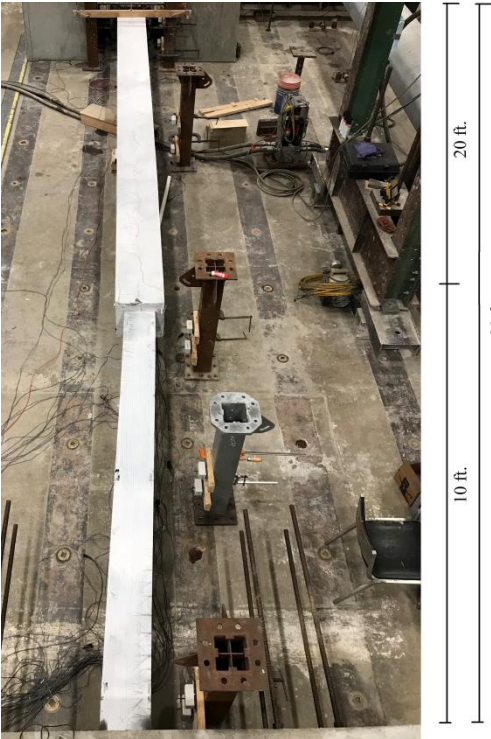
c) Fix section

**Figure 23. Displacement data from Specimen-2**

Similar to Specimen 1, the results indicated that the maximum transverse displacement occurred in section M.

3.5.3 Specimen-3 Test Results

Specimen-3 was 30 ft long with a 20 ft long concrete encasement. Figure 24-a shows the deformed shape of this specimen after buckling occurred.



a) Buckling of Specimen-3



b) Middle section (1)



c) Middle section (1)



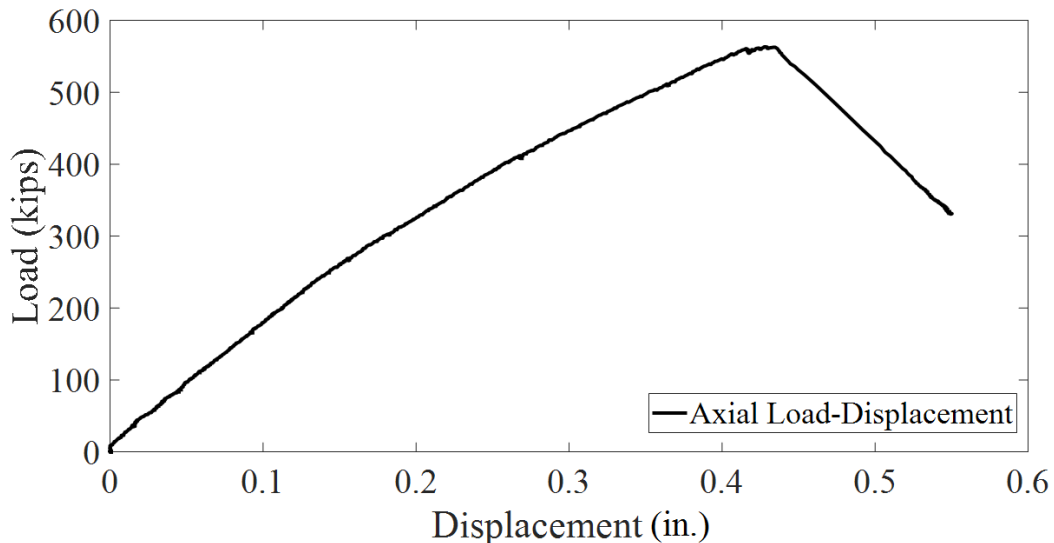
d) Fix section (1)

e) Fix section (1)

**Figure 24. Deformed shape of Specimen-3**

The maximum displacement occurred at the middle section, which was 20 ft 8in. from the pinned end of the pile. Similar to Specimen-2, longitudinal and transverse cracking were observed during the application of the load. Figure 24-b through -e show the deformed shape in sections M and F. As shown in Figure 24-b and -c, concrete crushing was observed at the end of the encasement near section M. Figure 24-d and -e show the condition of the pile at the fixed end. Based on this figure, no significant local buckling occurred at this location.

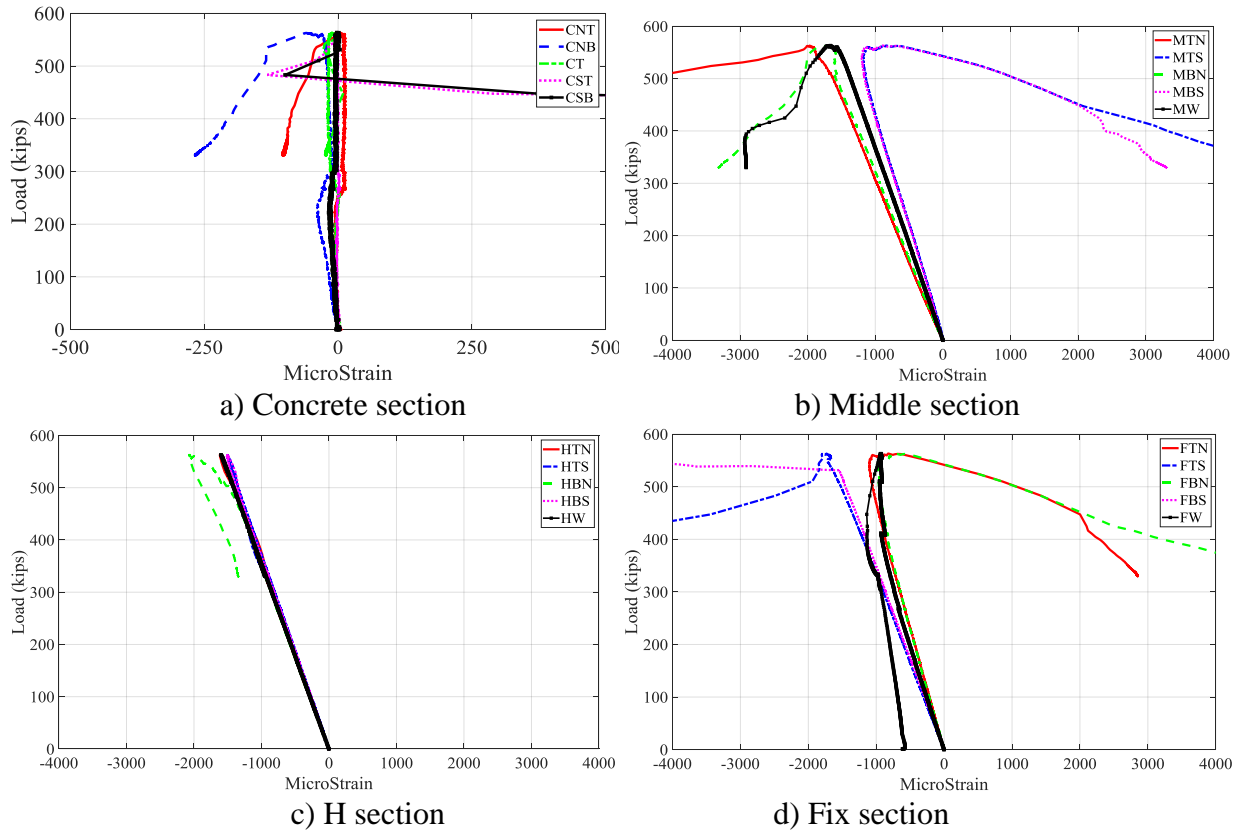
Figure 25 shows the axial load-displacement curve for Specimen-3. In this chart, by increasing the axial load, the axial displacement increased linearly until it reached the maximum load of 563 kips (620 kips for full cross-section yielding).



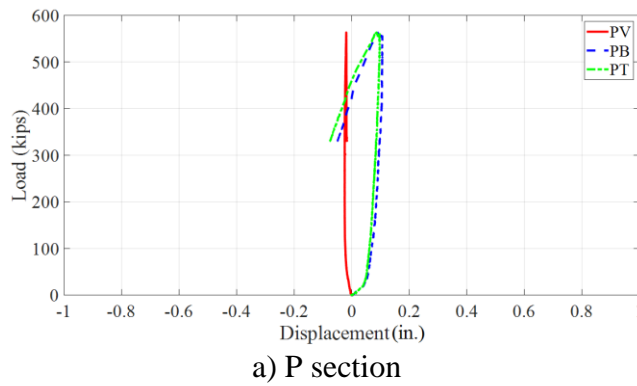
**Figure 25. Axial load-displacement of Specimen-3**

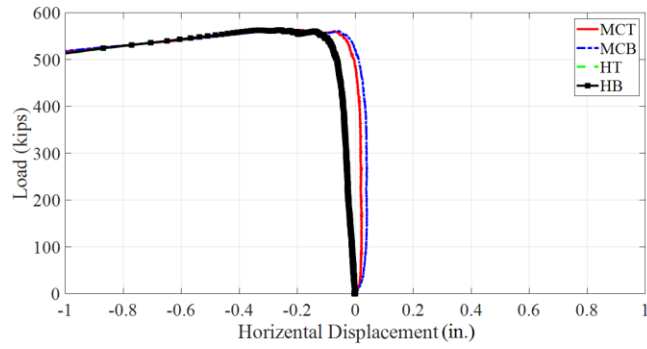
At this point, the pile experienced 0.4283 in. axial displacement. Similar to Specimen-2, the load displacement curve was not perfectly linear, again due to the cracking that occurred in the concrete encasement and the accompanying stiffness reduction.

Figure 26 and Figure 27 show the strain and displacement data, respectively, for Specimen-3.

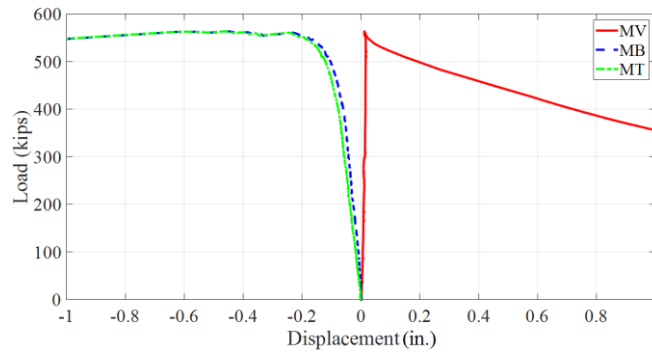


**Figure 26. Strain data from Specimen-3**

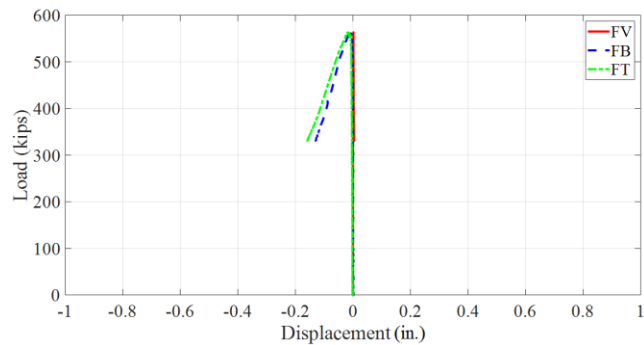




b) MC and H section



c) M section



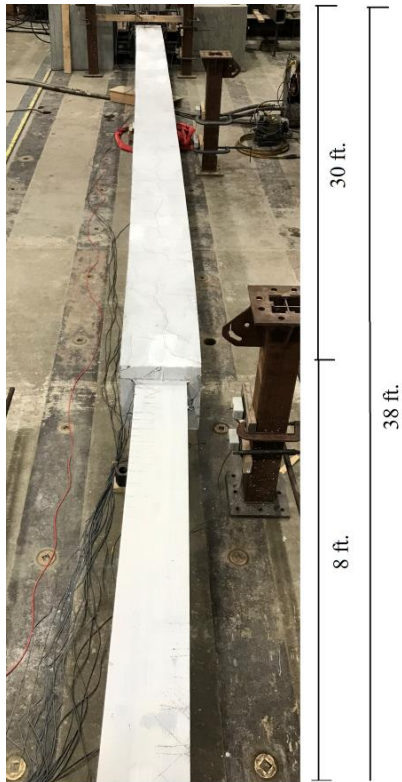
d) F section

**Figure 27. Displacement data from Specimen-3**

The data showed similar findings as those for Specimen-2. The strain results indicated that plasticity occurred in both sections M and F after the maximum load was reached.

### 3.5.4 Specimen-4 Test Results

Specimen-4 was 38 ft long with a 30 ft long concrete encasement. Figure 28 shows the deformed shape of this specimen after buckling occurred.



a) Buckling of Specimen-4



b) Middle section (1)



c) Middle section (2)



d) Fix section (1)

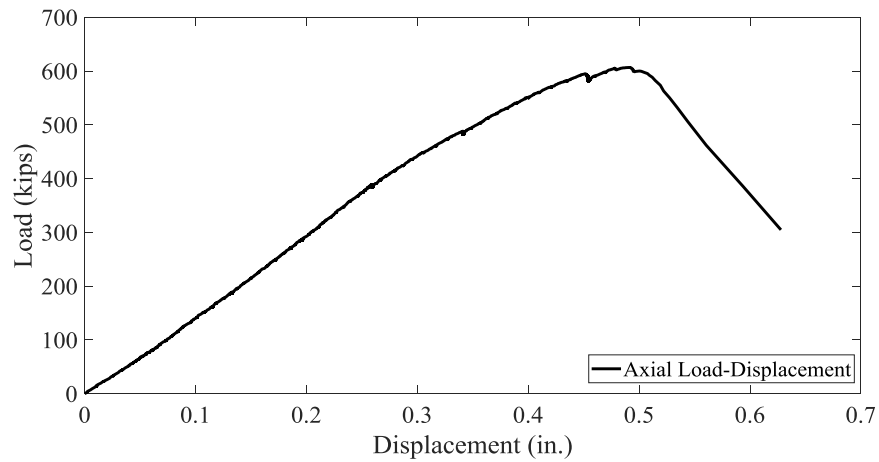


e) Fix section (2)

**Figure 28. Deformed shape of Specimen-4**

When the pile reached its maximum axial capacity, similar to the other specimens with encasements, it experienced bending toward the south side along its weak axis. The maximum displacement occurred at the middle section (30 ft 8 in. from the pinned end). Figure 28-b through -e show the deformation of the pile in the middle and fix sections. Similar to Specimen-2 and Specimen-3, longitudinal and transverse cracking were observed during the application of the load. In addition, concrete crushing occurred at the end of the encasement near the concrete section. On both sections M and F, the steel pile experienced significant strain.

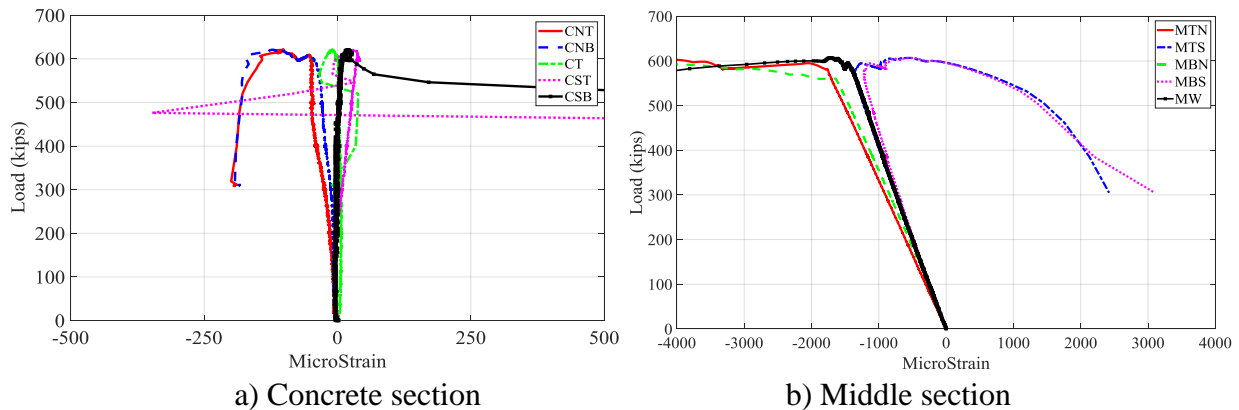
Figure 29 shows the axial load-displacement curve for Specimen-4.

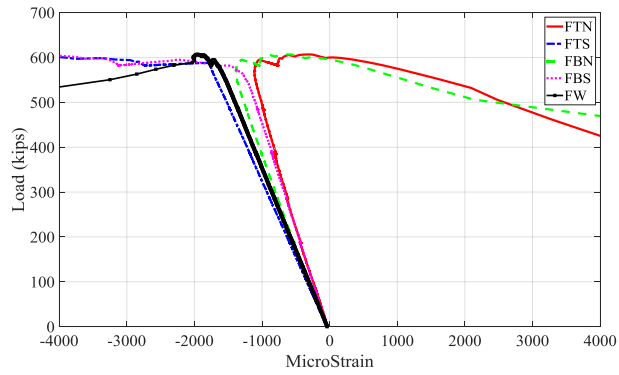


**Figure 29. Axial load-displacement of Specimen-4**

As the load increased, the axial displacement increased until it reached the maximum load of 606 kips (620 kips for full cross-section yielding). At this point, the pile experienced 0.4913 in. axial displacement. Similar to Specimen-2 and Specimen-3, the load displacement curve was not perfectly linear, again due to the cracking that occurred in the concrete encasement.

Figure 30 and Figure 31 show the strain and displacement data, respectively, for Specimen-4.





c) Fix section

**Figure 30. Strain data from Specimen-4**

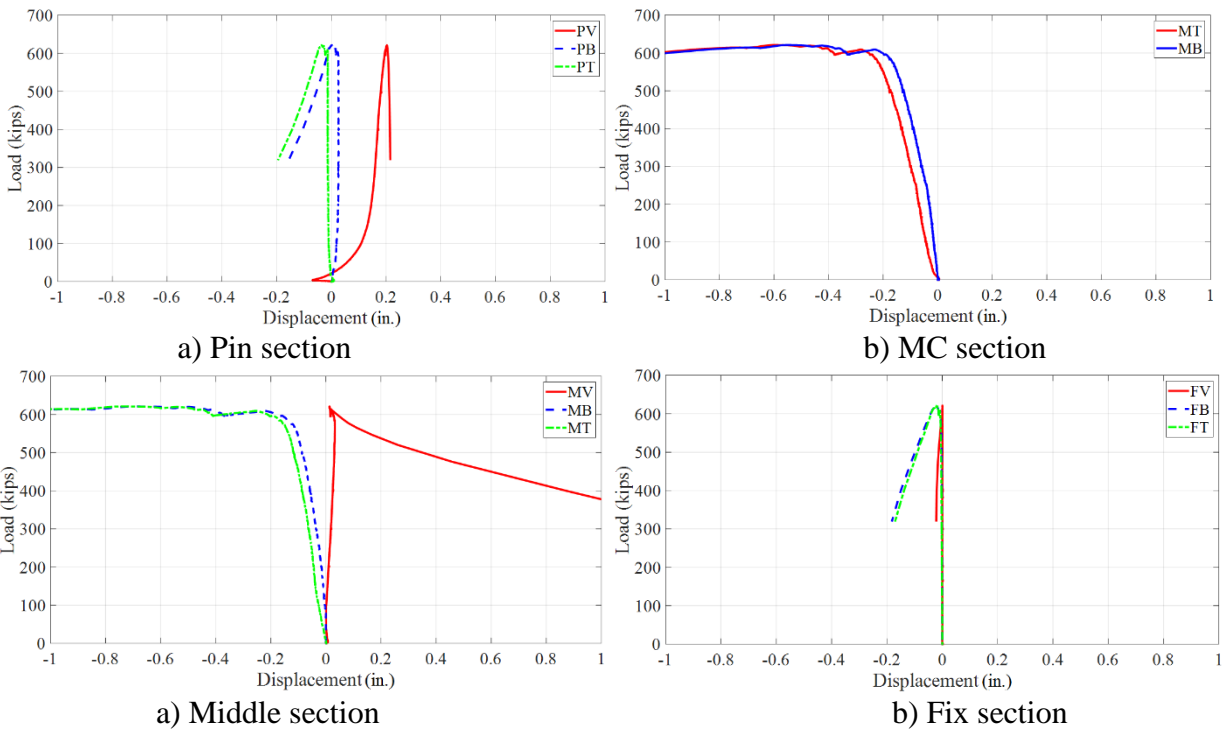


**Figure 31. Displacement data from Specimen-4**

The data showed similar findings to those for Specimen-3. The strain results indicated that plasticity occurred in both sections M and F after the load reached its maximum.

### 3.5.5 Results Summary

Figure 32 compares the axial load-displacements of the four specimens.

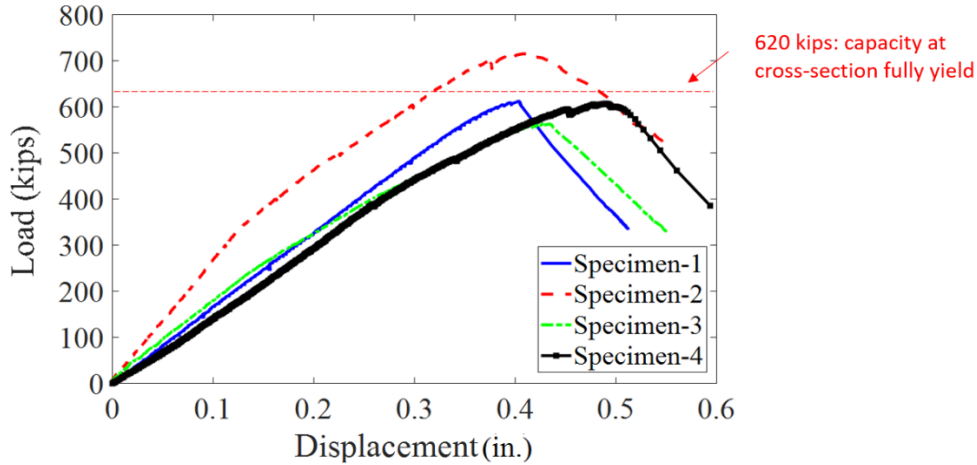


**Figure 32. Comparison of load-displacement from all specimens**

Comparing the results from Specimen-1 and Specimen-2, the chart shows that the concrete encasement increased the initial stiffness and maximum axial capacity of the pile. For Specimen-1 with no concrete encasement, the load-displacement was completely linear until it reached the critical buckling load. In the other three specimens, with encasements, the displacement curves were not perfectly linear. As mentioned previously, this was because cracking occurred in the concrete encasement and reduced the cross-sectional stiffness.

Table 7 provides additional comparisons between the buckling test results for the four specimens.

**Table 7. Experimental buckling test results for all specimens**

Specimen	Pile length (L) (ft)	Concrete encasement length (L <sub>c</sub> ) (ft)	Ratio (L <sub>c</sub> /L) –	Buckling load (kips)	Buckling displacement (in.)
Specimen-1	16	0	0	612	0.4013
Specimen-2	16	10	0.625	715	0.4087
Specimen-3	30	20	0.667	563	0.4283
Specimen-4	38	30	0.789	606	0.4913

Based on the data in this table, Specimen-1 and Specimen-2 showed a similar axial displacement when buckling occurred. However, the maximum capacity of Specimen-2 was 715 kips (about 103 kips higher than that of Specimen-1) given its concrete encasement. Although Specimen-4 was longer than Specimen-3, it showed a higher maximum capacity than Specimen-3. This is because of the concrete encasement. The ratio of length of encasement over total length (L<sub>c</sub>/L) for Specimen-3 was less than that for Specimen-4. These results indicate that the concrete encasement contributes significantly to the capacity of the pile.

## CHAPTER 4. ASSESSMENT TOOL VALIDATION

In the present study, four pile specimens were selected to compare their experimental axial capacity with values that the assessment tool predicts. Table 8 provides a comparison between the experimental buckling strength found in the laboratory and the values calculated utilizing the previously created assessment tool along with AISC equation results. The AISC equation ignores the contribution of the concrete encasement.

**Table 8. Comparison between experimental and assessment tool results**

Specimen	Experimental (kips)	Assessment tool		AISC equation	
		Result (kips)	Difference (%)	Result (kips)	Difference (%)
Specimen-1	612	493	24	493	24
Specimen-2	715	606	18	493	46
Specimen-3	563	521	8	278	102
Specimen-4	606	556	9	179	238

The results indicate that the assessment tool predicts the capacity of the pile about 8% to 24% lower than the experimental results, so provides a conservative approach. In general, the assessment tool results are more conservative for the pile without encasement than that for the encased pile. Comparing the results between the experimental tests and AISC equations, the results indicated that the AISC equations predict the capacity of the pile about 24% to 238% less than the results from the experimental tests. This significant difference is caused by ignoring the contribution of the concrete encasements.

## CHAPTER 5. SUMMARY AND CONCLUSIONS

Concrete encasements are utilized to protect bridge piles from corrosion and environmental stressors. However, the contributions of concrete encasements are not currently considered in the design of piles for capacity considerations in Iowa. Additionally, rating engineers need to have realistic evaluation methods for piles to estimate the capacity of the foundation for scour-critical bridges following scour events. For this reason, a rapid assessment tool was developed in the Phase I research to calculate the capacity of concrete encased piles.

This rapid pile assessment tool was developed and verified using theoretical modeling approaches. However, experimental data to validate the tool's results were not available or part of the scope of that work. The goal of this research project was to validate the previously developed rapid pile assessment tool's findings to ensure accurate pile capacity determination, both for bare piles and those encased in concrete.

To achieve this goal, four specimens with various lengths and concrete encasement lengths and ratios were constructed and tested via axial loading in the laboratory. All specimens were HP 10×42 cross-sections (with various lengths). The first and second specimens were 16 ft long while the third and fourth specimens were 30 ft and 38 ft long, respectively. The first specimen had no concrete encasement and the length of encasement for the second, third, and fourth specimens were 10, 20, and 30 ft, respectively.

The specimens were tested in a pin-fixed boundary condition without any eccentricity. The results from the experimental tests were compared with the predictions from the assessment tool. These were the key findings:

- The pile assessment tool provides a conservative estimation of the axial capacity of the piles. The prediction results were about 8% to 24% lower than those from the experimental results.
- Concrete encasement increases the initial axial stiffness of the piles.
- Concrete encasement has a significant effect on the axial capacity of the steel HP piles. However, this contribution is ignored in current design procedures.
- Ignoring the effect of the concrete encasement, as with the use of the equations suggested by the AISC, can result in a significantly conservative prediction.

In summary, the previously developed pile capacity assessment tool was validated through the experimental results and still provides a conservative estimation of pile capacity for concrete encased piles. While providing conservative results, the capacities resulting from the tool are significantly higher than those obtained using AISC specifications. As such, valuable additional capacity can be seen when including the contribution from concrete encasements.

Additional research should be conducted on pile encasement for piles encased in circular concrete sections. The Iowa DOT plans typically allow such a replacement in shape at the contractor's discretion. To ensure full usefulness of the capacity estimation tool, the tool should be updated to include circular cross-sections and subsequently verified experimentally.

Another research direction focusing on investigating the benefits in design for a fully encased pile bent is recommended. The current practice of designing the fully encased pile bent pier is to place the weak axis of the pile parallel to the bridge longitudinal direction. Since the concrete encasement significantly increases the capacity of the pile, it would be interesting to study the benefits to rotate the pile 90° and place it with weak axis of the pile perpendicular to the longitudinal bridge direction. The potential benefits of doing this may increase the moment capacity (about the bridge transverse direction) of the pier and eventually reduce the number of piles required.

## REFERENCES

- Ainge, S. W. 2012. *Repair and Strengthening of Bridge Substructures*. MS thesis. Marquette University, Milwaukee, WI.
- ACI 318. 2014. *Building Code Requirements for Structural Concrete and Commentary*. American Concrete Institute, Farmington Hills, MI.
- AISC. 2017. *AISC Steel Construction Manual*, 15th Edition. American Institute of Steel Construction, Chicago, IL.
- ASTM. 2018. *ASTM C39: Standard Test Method for Compressive Strength of Cylindrical Concrete Specimens*. ASTM International, West Conshohocken, PA.
- AASHTO. 2012. *AASHTO LRFD Bridge Design Specifications*. American Association of State Highway and Officials, Washington, DC.
- Castilla, F., P. Martin, and J. Link. 1984. *Fixity of Members Embedded in Concrete*. Army Construction Engineering Research Laboratory, Champaign, IL.
- Deng, Y. (“J.”), B. M. Phares, and P. Lu. 2018. *Development of a Rapid Assessment Tool for Pile Capacity and Stability in Response to Scour Situations*. Bridge Engineering Center, Iowa State University, Ames, IA.  
[https://intrans.iastate.edu/app/uploads/2018/03/pile\\_assessment\\_tool\\_w\\_cvr.pdf](https://intrans.iastate.edu/app/uploads/2018/03/pile_assessment_tool_w_cvr.pdf).
- Fischenich, C. and M. Landers. 2000. *Computing Scour*. Technical Note. U.S. Army Corps of Engineers Ecosystem Management and Restoration Research Program.
- Hughes, D., G. E. Ramey, and M. L. Hughes. 2007a. Bridge Pile Bent Number of Piles and X-Bracing System: Impact on Pushover Capacity as Scour Increases. *Practice Periodical on Structural Design and Construction*, Vol. 12, No. 2, pp. 82–95.
- . 2007b. Effects of Extreme Scour and Soil Subgrade Modulus on Bridge Pile Bent Buckling. *Practice Periodical on Structural Design and Construction*, Vol. 12, No. 2, pp. 96–108.
- Iowa DOT. 2019. *LRFD Concrete and Steel Trestle Pile Bents-PI0L*. Iowa Department of Transportation, Bridges and Structures Bureau, Ames, IA.  
<https://iowadot.gov/bridge/bridge-and-culvert-standards/bridge-standards>.
- . 2021. *LRFD Bridge Design Manual*. Iowa Department of Transportation, Bridges and Structures Bureau, Ames, IA.
- Kattell, J. and M. Eriksson. 1998. *Bridge Scour Evaluation: Screening, Analysis, and Countermeasures*. USDA Forest Service, San Dimas Technology and Development Center, San Dimas, CA.
- Lagasse, P. F., P. E. Clopper, L. W. Zevenbergen, and L. G. Girard. 2007. *NCHRP Report 593: Countermeasures to Protect Bridge Piers from Scour*. National Cooperative Highway Research Program, Washington, DC.
- Lampo, R., T. Nosker, D. Barno, J. Busel, A. Maher, P. Dutta, and R. Odello 1998. *Development and Demonstration of FRP Composite Fender, Load-Bearing, and Sheet Piling Systems*. US Army Corps of Engineers, Construction Engineering Research Laboratories, Champaign, IL.
- Liang, F., C. R. Bennett, R. L. Parsons, J. Han, and C. Lin. 2009. A Literature Review on Behavior of Scoured Piles under Bridges. International Foundation Congress and Equipment Expo 2009, March 15–19, Orlando, FL. *Contemporary Topics in In Situ Testing, Analysis, and Reliability of Foundations*, pp. 482–489.

- Liang, F., H. Zhang, and M. Huang. 2015. Extreme Scour Effects on the Buckling of Bridge Piles Considering the Stress History of Soft Clay. *Natural Hazards*, Vol. 77, No. 2, pp. 1143–1159.
- Lin, C., C. Bennett, J. Han, and R. L. Parsons. 2012. Integrated Analysis of the Performance of Pile-Supported Bridges under Scoured Conditions. *Engineering Structures*, Vol. 36, pp. 27–38.
- Lin, C., J. Han, C. Bennett, and R. L. Parsons. 2014. Case History Analysis of Bridge Failures Due to Scour. International Symposium of Climatic Effects on Pavement and Geotechnical Infrastructure 2013, August 4–7, Fairbanks, AK. *Climatic Effects on Pavement and Geotechnical Infrastructure*, pp. 204–216.
- Salmon, C. G. and J. E. Johnson. 1996. *Steel Structures: Design and Behavior: Emphasizing Load and Resistance Factor Design*. Harper Collins, New York, NY.
- Wardhana, K. and F. C. Hadipriono. 2003. Study of Recent Building Failures in the United States. *Journal of Performance of Constructed Facilities*, Vol. 17, No. 3, pp. 151–158.
- Zhang, G., S. A. Hsu, T. Guo, X. Zhao, A. D. Augustine, and L. Zhang. 2013. *Evaluation of Design Methods to Determine Scour Depths for Bridge Structures*. Louisiana Transportation Research Center, Baton Rouge, LA.



**THE INSTITUTE FOR TRANSPORTATION IS THE FOCAL POINT FOR TRANSPORTATION  
AT IOWA STATE UNIVERSITY.**

**InTrans** centers and programs perform transportation research and provide technology transfer services for government agencies and private companies;

**InTrans** contributes to Iowa State University and the College of Engineering's educational programs for transportation students and provides K–12 outreach; and

**InTrans** conducts local, regional, and national transportation services and continuing education programs.



**IOWA STATE  
UNIVERSITY**

Visit [InTrans.iastate.edu](http://InTrans.iastate.edu) for color pdfs of this and other research reports.